Transversal homoclinic orbits in a transiently chaotic neural network

Shyan-Shiou Chen and Chih-Wen Shih

Citation: Chaos: An Interdisciplinary Journal of Nonlinear Science **12**, 654 (2002); doi: 10.1063/1.1488895
View online: http://dx.doi.org/10.1063/1.1488895
View Table of Contents: http://scitation.aip.org/content/aip/journal/chaos/12/3?ver=pdfcov
Published by the AIP Publishing

Transversal homoclinic orbits in a transiently chaotic neural network

Shyan-Shiou Chen and Chih-Wen Shih[a)]
Department of Applied Mathematics, National Chiao Tung University, Hsinchu, Taiwan, Republic of China

(Received 29 October 2001; accepted 7 May 2002; published 15 August 2002)

We study the existence of snap-back repellers, hence the existence of transversal homoclinic orbits in a discrete-time neural network. Chaotic behaviors for the network system in the sense of Li and Yorke or Marotto can then be concluded. The result is established by analyzing the structures of the system and allocating suitable parameters in constructing the fixed points and their pre-images for the system. The investigation provides a theoretical confirmation on the scenario of transient chaos for the system. All the parameter conditions for the theory can be examined numerically. The numerical ranges for the parameters which yield chaotic dynamics and convergent dynamics provide significant information in the annealing process in solving combinatorial optimization problems using this transiently chaotic neural network. © *2002 American Institute of Physics.*
[DOI: 10.1063/1.1488895]

Artificial neural networks mimic the features of real biological neurons in certain aspects such as linear additivity for the inputs and strong nonlinearity for the resulting output. Many individual biological neurons are known to fire chaotic signals. Coupling an assembly of these chaotic neurons results in various kinds of dynamical phenomena. This investigation proposes a new analytical method to detect chaotic behaviors in a coupled artificial neural network system. A construction scheme for transversal homoclinic orbits in neighborhoods of repelling fixed points for the system is developed. We first analyze the basic structures of the corresponding one-dimensional single-neuron maps. With suitable formulations on these one-dimensional maps, the constructions for pre-images of the fixed points, hence homoclinic orbits, are implemented by the standard Brouwer's fixed point theorem. The approach is natural mathematically, as one attempts to obtain the information on orbits in multidimensional phase space from the one in low dimension (one-dimension herein). We also address some convergence theorem for the system, which is usually necessary in the applications of neural networks. The whole system thus exhibits both chaotic and convergent dynamics as the self-feedback connection weights vary. This theoretical study not only confirms these dynamics but also provides more detailed scenario of the chaotic behaviors for the network. Moreover, establishing the computable conditions which result in these dynamics contributes toward the applications of the neural networks.

I. INTRODUCTION

Artificial neural networks have been applied to solve many information processing and combinatorial optimization problems with considerable success.[1–5] In using the networks as computational methods to solve combinatorial optimization problems, chaotic behaviors for the system can provide global searching ability which prevents the objective function from getting trapped at local extrema.[6,7] In this investigation, we plan to study the chaotic behaviors in a discrete-time neural network, called transiently chaotic neural network (TCNN) which was proposed by Chen and Aihara.[6–8] The model of TCNN can be described by the following equations: for $i=1,\ldots,n$,

$$x_i(t+1)=\alpha x_i(t)+\omega_{ii}(t)(y_i(t)-a_{0i})+\sum_{j=1,j\neq i}^{n}\omega_{ij}y_j(t)+a_i, \tag{1.1}$$

$$y_i(t)=(1+e^{[-x_i(t)/\varepsilon]})^{-1}, \tag{1.2}$$

$$|\omega_{ii}(t+1)|=(1-\gamma)|\omega_{ii}(t)|. \tag{1.3}$$

Here, x_i is the internal state of neuron i; y_i is the output of neuron i; α is the damping factor; ω_{ii} is the self-feedback connection weight; a_{0i} is self-recurrent bias of neuron i; ω_{ij} is the connection weight from neuron j to neuron i; a_i is the input bias of neuron i; ε is the steepness parameter of the output function; γ is the damping factor (a fixed number with $0<\gamma<1$). Equation (1.3) represents an exponential cooling schedule in the annealing procedure.[6]

The TCNN is a discrete-time analogue of classical neural network models. Classical deterministic neural networks are continuous-time models.[1,2] Most of these models possess gradient-like structures. Hopfield and Tank[3] have adopted such a continuous-time model to solve certain optimization problems. Recently, it has been shown that the discrete-time model TCNN has better global searching ability. Chaotic ingredients of TCNN prevent the iterations from getting trapped at local extreme points of the objective function for the application problems. The TCNN admits chaotic behaviors for certain parameters as well as asymptotic convergence to fixed points for some other parameters. One can then tune the parameter (for example, the so-called temperature in the annealing process) to obtain better solutions.[5,6]

We shall investigate the existence of snap-back repellers for the TCNN. The existence of snap-back repellers implies the existence of transversal homoclinic orbits. Certain sense

[a)]Author to whom correspondence should be addressed. Electronic mail: cwshih@math.nctu.edu.tw

of chaos can then be concluded, according to the theorem by Marotto,[9] see also Ref. 10. Marotto's theorem generalized the results by Li and Yorke[11] on chaotic behaviors in one-dimensional difference equations to the ones in multidimensional systems. This theorem, as quoted in Appendix C, indicates that with the presence of snap-back repeller, the phase space possesses a topological structure which includes infinitely many periodic points and a scrambled set. Very erratic behaviors of the system then occur, including the lack of global stability for solutions, and the existence of an uncountable collection of orbits which do not eventually approach any periodic points.

There is a considerable computational difficulty in determining the existence of snap-back repellers of multidimensional systems. Such difficulty arises from the unstable structures of the dynamics for the system. For TCNN (1.1)–(1.3), the convergence of dynamics and the chaotic behavior in the sense of Marotto have been studied in Refs. 7 and 8. The results therein on the existence of snap-back repellers are under several assumptions on the parameters. One of the crucial conditions is that ω_{ii}, the self-feedback connection weight, has to be large enough. In fact, their arguments involve taking ω_{ii} to infinity. This is due to the uses of a mathematical technique, namely, the Urabe's proposition. With our approach, all the parameter conditions are explicit and can be examined numerically. Substantial parts of the regime of chaos and the regime of convergence can then be concluded theoretically, as shown in Secs. IV and V.

We shall analyze the existence of snap-back repellers by making use of certain structures in the corresponding one-dimensional maps. Based on the formulation for these maps, the parameter ranges for the existence of fixed points can be determined and the pre-images of these fixed points can be constructed, in the multidimensional systems. These pre-images form the homoclinic orbits for the respective fixed point. Our constructions actually indicate the existence of infinitely many homoclinic orbits for a single snap-back repeller. Hence, the investigation also provides more detailed scenario of dynamics for the system. Moreover, our results are not limited to the dimensions of the problems. As for the investigations in utilizing suitable low dimensional maps to study high dimensional maps, Marotto[12] presented a scheme to study two-dimensional problems by perturbing related scalar equations. That result has been applied to prove the existence of transversal homoclinic orbit for the Hénon map.[13] However, not all feasible perturbations were estimated in these works.

TCNN system (1.1)–(1.3) may not be chaotic. In fact, for certain parameters, the system settles at steady states as time tends to infinity. Restated, every orbit of the system tends to a fixed point.[14] Our result in Sec. V is related to such dynamical properties. To study the transiently chaotic behaviors of the system, we shall analyze the dynamics of TCNN at fixed self-feedback connection weight. Namely, instead of considering (1.1)–(1.3), we shall analyze dynamics of the following iteration map:

$$x_i(t+1)=\alpha x_i(t)+\omega_{ii}(y_i(t)-a_{0i}) + \sum_{j=1,j\neq i}^{n} \omega_{ij}y_j(t)+a_i . \tag{1.4}$$

That is, by setting ω_{ii} to constants, we study the behaviors of (1.4) for different parameters, including ω_{ii}, as the approach in Refs. 7 and 8. (1.1)–(1.3) can be regarded as a skew system of (1.4) over (1.3).[15,16] There is a dynamical correspondence between iterations of (1.1)–(1.3) and evolutions of (1.4) away from the parameters at bifurcation values.

The existence of snap-back repellers and the construction of transversal homoclinic orbits for TCNN are the main exposition of this work. For application purpose, we intend to present our results within the complete set of parameters in the original model. The analysis and parameter conditions for these discussions in Secs. III and IV are rather involved. Therefore, we plan to sketch these ideas in a simplified situation in Sec. II. In Sec. III, we formulate a one-dimensional map which is analogous to the single neuron map. Several lemmas to be used in the later sections are derived. The existence of snap-back repellers for multidimensional TCNN (1.4) will be discussed in Sec. IV. In Sec. V, we generalize the result on the existence of a Lyapunov function for (1.4) from symmetric connection weights[8] to cycle-symmetric ones.[17] Precise statements on convergence to fixed points of the system will also be addressed. In addition, the parameter conditions for the existence of Lyapunov function and those for the existence of snap-back repellers are compared. In Sec. VI, we shall provide several numerical illustrations on the parameter ranges and computations of the Lyapunov exponent for the parameters in the chaotic regime. Some proofs of the lemmas and proposition in Sec. III are given in Appendix A. The statements of the Gerschgorin's theorem and the Marotto's theorem are quoted in Appendixes B and C, respectively.

II. ILLUSTRATIONS OF SNAP-BACK REPELLERS FOR TCNN

We shall sketch the ideas of finding snap-back repellers and constructing pre-images of repellers for TCNN in this section. Detailed analysis and precise statements with verifications will be given in Secs. III and IV.

According to the definition of snap-back repeller for a map F (see Appendix C), to assure that a repeller $\overline{X}$ is a snap-back repeller, we have to find a neighborhood $B(\overline{X};r)$ of $\overline{X}$ such that all eigenvalues of $DF(X)$, $X\in B(\overline{X};r)$, exceed unity in norm, and a point $X_0\in B(\overline{X};r)$ (called snap-back point) such that $F^m(X_0)=\overline{X}$ and $\det(DF^m(X_0))\neq 0$ for some positive integer m. If this is the case, then one of the orbits through X_0 is a transversal homoclinic orbit for the map.

We start our illustrations of snap-back repellers from some one-dimensional unimodal maps in Fig. 1. We assume that the slopes at $\overline{X}$ for the mappings in Fig. 1 all have their absolute values greater than one. Thus $\overline{X}$ is a repeller for every graph of Fig. 1. Notice that certain backward orbit of $\overline{X}$

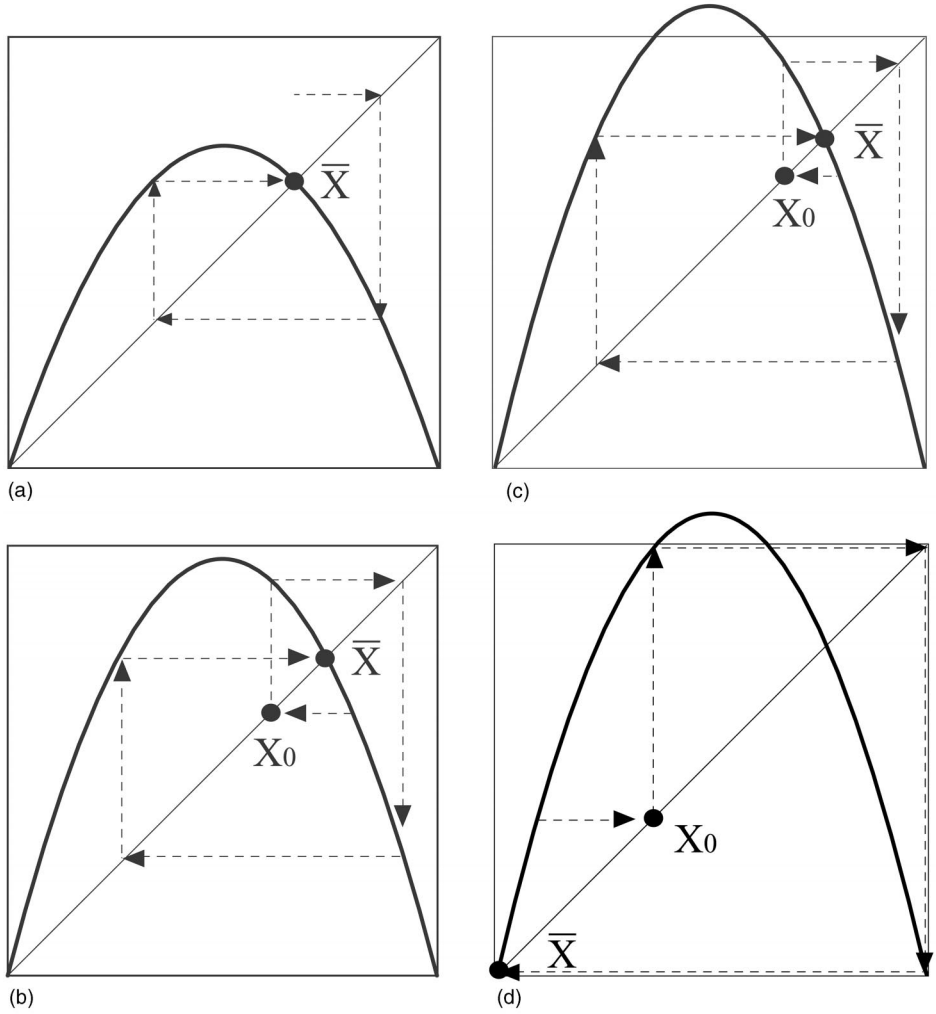

FIG. 1. With X_0 as a snap-back point, fixed point $\overline{X}$ is a snap-back repeller in (b), (c), (d), but not in (a).

enters into a neighborhood of $\overline{X}$, in (b), (c), and (d) of Fig. 1. Therefore, $\overline{X}$ is a snap-back repeller in (b), (c), and (d) of Fig. 1, if further condition on the slope of the map in a neighborhood of $\overline{X}$ is imposed. In (a) of Fig. 1, one simply cannot find points in the backward orbits of $\overline{X}$, which lie in a unstable neighborhood of $\overline{X}$.

Let us consider the one-dimensional TCNN. For $n=1$, (1.4) becomes

$$F(x)=\alpha x+\omega g_{a_0}(x)+a, \tag{2.1}$$

where $g_{a_0}(x):=(1+e^{-x/\varepsilon})^{-1}-a_0$. Here, to avoid complication from the parameters, one may simply take the parameter values as $a=0$, $\alpha=-2.5$, $\omega=50$, $a_0=0.5$, $\varepsilon=1$. The graph of such F is depicted in Fig. 2. We locate the points p_1,p_2,p_3,p_4 where $F'(p_1)=F'(p_3)=-1$, and $F'(p_2)=F'(p_4)=1$. Moreover, it can be computed that $F'(x)>1$ if $x\in\tilde{\Omega}^{\mathrm{m}}:=\{x:p_4<x<p_2\}$, and $F'(x)<-1$ if $x\in\tilde{\Omega}^{l}:=\{x:x<p_3\}$ or $x\in\tilde{\Omega}^{\mathrm{r}}:=\{x:x>p_1\}$. Notably, F has three fixed points $\overline{x}_l\in\tilde{\Omega}^{l},\overline{x}_{\mathrm{m}}\in\tilde{\Omega}^{\mathrm{m}}$, and $\overline{x}_{\mathrm{r}}\in\tilde{\Omega}^{\mathrm{r}}$ ("l," "m," "r" are as left, middle, right). The pre-images of each of these fixed points will be constructed also in these regions. In doing so, on the one hand, we always have $|F'(x)|>1$ for any point x in these regions. On the other hand, $DF^m(X_0)\neq 0$, if X_0 is the constructed snap-back point for the fixed point with $F^m(X_0)=\overline{x}_l$, or $\overline{x}_{\mathrm{m}}$, or $\overline{x}_{\mathrm{r}}$. Notably, F in shaded areas in Fig. 2 reads as two unimodal maps glued together. Though the left-lower part is upside-down, pre-images for fixed points $\overline{x}_l$ and $\overline{x}_{\mathrm{m}}$ under F can be found in a manner analogous and symmetric to the ones in Figs. 1(c) and 1(d), re-

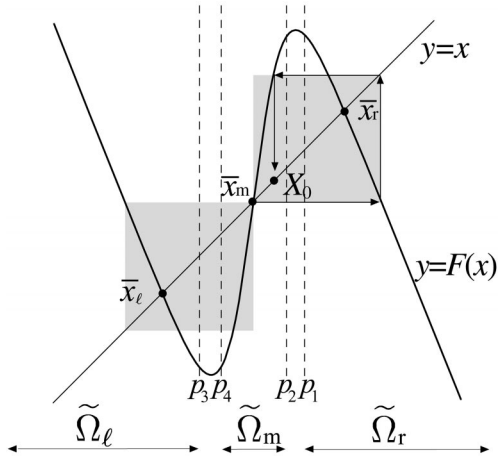

FIG. 2. One-dimensional TCNN with $a=0$, $\alpha=-2.5$, $\omega=50$, $a_0=0.5$, $\varepsilon=1$.

spectively. In the right-upper part, finding pre-images for fixed points $\overline{x_r}$ and $\overline{x_m}$ under F are exactly the same as in Figs. 1(c) and 1(d), respectively. We note that F is not symmetric to the origin. Therefore, the configurations of F on the right-hand side and the left-hand side need to be considered separately, as far as the parameter conditions are concerned.

In general discussions in Sec. III, the properties for the slopes of F and these separating points p_1-p_4 will be assured by condition (PC-1-a) or (PC-2-a). The graph in Fig. 2 can be shifted upward or downward without changing these slope properties. Thus, one certainly needs conditions [(PC-1-b) or (PC-2-b) in Sec. III] to guarantee the existence of fixed points for F at proper locations. To construct pre-images for each of the fixed points $\overline{x_l},\overline{x_m},\overline{x_r}$, appropriate configurations are required for the graph of F. For instance, $F(p_1)$ and $F(p_2)$ should be larger than $F(X_0)$ and one should avoid the situation like Fig. 1(a) in right-upper shaded part or left-lower shaded part of F in Fig. 2. Conditions (PC-1-c) or (PC-2-c) in Sec. III are responsible for such requirements, though they are actually formulated for a family of one-dimensional TCNNs.

Now let us consider the two-dimensional TCNN. Let $\mathbf{x}=(x_1,x_2)$, $F(x_1,x_2)=(F_1(x_1,x_2),\ F_2(x_1,x_2))$. Equation (1.4) with $n=2$ becomes

$$F_1(x_1,x_2)=\alpha x_1+\omega g_\rho(x_1)+\omega_{12}g_0(x_2),$$

$$F_2(x_1,x_2)=\alpha x_2+\omega g_\rho(x_2)+\omega_{21}g_0(x_1).$$

Here, $g_0(x)=(1+e^{-x/\varepsilon})^{-1}$ and for simplicity, we set $\rho=a_{01}=a_{02}$, $a_1=a_2=0$. To avoid complication from parameters, one can take the parameter values as $\alpha=-2.5$, $\omega=50$, $\rho=0.5$, $\varepsilon=1$ again.

Analogous to the one-dimensional case, we need to know the eigenvalue properties of $DF(\mathbf{x})$ for $\mathbf{x}$ in the phase plane. Notably,

$$DF(x_1,x_2)=\begin{pmatrix}\alpha+\omega g_\rho'(x_1) & \omega_{12}g_0'(x_2)\\ \omega_{21}g_0'(x_1) & \alpha+\omega g_\rho'(x_2)\end{pmatrix}. \tag{2.2}$$

Since $|g_0'|\leqslant 1/4\varepsilon$, by Gerschgorin's theorem, the eigenvalues of $DF(x_1,x_2)$ will have their norms greater than one if $|\alpha+\omega g_\rho'(x_1)|>1+(k/4\varepsilon)$, and $|\alpha+\omega g_\rho'(x_2)|>1+(k/4\varepsilon)$, where $k=\max\{|\omega_{12}|,|\omega_{21}|\}$. On the other hand, since $0<g_0<1$, the following inequalities hold for all x_1, x_2:

$$\check{f}(x_1)\leqslant F_1(x_1,x_2)\leqslant\hat{f}(x_1), \tag{2.3}$$

$$\check{f}(x_2)\leqslant F_2(x_1,x_2)\leqslant\hat{f}(x_2), \tag{2.4}$$

where, for $x\in\mathbb{R}$, $\check{f}(x):=\alpha x+\omega g_\rho(x)-k$ and $\hat{f}(x):=\alpha x+\omega g_\rho(x)+k$. One then performs similar process on $\check{f}$, $\hat{f}$ as in one-dimensional case. To obtain eigenvalue properties of $DF(\mathbf{x})$ mentioned following (2.2), we locate the points p_1, p_2, p_3, p_4, so that the slopes of $\check{f}$ (and $\hat{f}$) at these points are either $1+(k/4\varepsilon)$ or $-1-(k/4\varepsilon)$. Under further condition [(PC-1-b) or (PC-2-b) in Sec. III], for every h with $-k\leqslant h\leqslant k$, $f_h(x):=\alpha x+\omega g_\rho(x)+h$ (hence $\check{f}\leqslant f_h\leqslant\hat{f}$) has three fixed points in suitable regions. Accordingly, for any fixed $x_2=\xi_2\in\mathbb{R}$ (respectively, any fixed $x_1=\xi_1\in\mathbb{R}$), take $\omega_{12}g_0(\xi_2)$ [respectively, $\omega_{21}g_0(\xi_1)$] as h. Then the one-dimensional map $f_h(x)=F_1(x,\xi_2)$ [respectively, $f_h(x)=F_2(\xi_1,x)$] has a fixed point in each of the three regions $\tilde{\Omega}^l,\tilde{\Omega}^m,\tilde{\Omega}^r$. Herein, these three regions correspond to the parameters α, ω, ρ, ε, k in the one-dimensional map $\hat{f}$. With these properties, it can be shown that there exist nine $(3^n,\ n=2)$ fixed points $\overline{\mathbf{x}}_{**}$, ''$*$'',''$\star$''$\in\{l,\mathrm{m},\mathrm{r}\}$, of the two-dimensional map F, using the Brouwer's fixed point theorem. Each of the nine regions Ω_{**} contains exactly one of these fixed points. (See Fig. 3.)

For constructions of the pre-images for each of these fixed points, we again utilize the formulations of the one-dimensional maps $\{f_h\}$. Let us illustrate the construction for the middle fixed point $\overline{\mathbf{x}}_{\mathrm{mm}}\in\tilde{\Omega}_{\mathrm{mm}}$. Write $\overline{\mathbf{x}}_{\mathrm{mm}}=(\overline{x_1},\overline{x_2})$. Consider the equations $F_1(x_1,x_2)=\overline{x_1}$, $F_2(x_1,x_2)=\overline{x_2}$, that is,

$$\alpha x_1+\omega g_\rho(x_1)+\omega_{12}g_0(x_2)=\overline{x_1}, \tag{2.5}$$

$$\alpha x_2+\omega g_\rho(x_2)+\omega_{21}g_0(x_1)=\overline{x_2}. \tag{2.6}$$

Let us work on the left-lower region in Fig. 4. For any fixed $x_2=\xi_2\in\mathbb{R}$, the graph of $f_h(x)=F_1(x,\xi_2)$ intersects the horizontal line $y=\overline{x_1}$ at two points $x_1^{-1,\mathrm{m}}$, $x_1^{-1,l}$ (see Fig. 4). Similarly, for any fixed $x_1=\xi_1\in\mathbb{R}$, the graph of $f_h(x)=F_2(\xi_1,x)$ intersects the horizontal line $y=\overline{x_2}$ at two points $x_2^{-1,\mathrm{m}}$, $x_2^{-1,l}$. Restated, for any fixed (ξ_1,ξ_2), there correspond four points $(x_1^{-1,l},x_2^{-1,l})$, $(x_1^{-1,l},x_2^{-1,\mathrm{m}})$, $(x_1^{-1,\mathrm{m}},x_2^{-1,l})$, and $(x_1^{-1,\mathrm{m}},x_2^{-1,\mathrm{m}})$, which belong to $\tilde{\Omega}_{ll}$, $\tilde{\Omega}_{l\mathrm{m}}$, $\tilde{\Omega}_{\mathrm{m}l}$, and $\tilde{\Omega}_{\mathrm{mm}}$, respectively. It follows that four mappings are produced. Namely, $H:(\xi_1,\xi_2)\to(x_1^{-1,*},x_2^{-1,\star})$, where $(*,\star)=(l,l),(l,\mathrm{m}),(\mathrm{m},l),(\mathrm{m},\mathrm{m})$. A fixed point $(\overline{x_1}^{-1,*},\overline{x_2}^{-1,\star})$ for each one of these mappings H gives a solution to (2.5), (2.6), and hence a pre-image of $\overline{\mathbf{x}}_{\mathrm{mm}}$ under F. Notably, $(\overline{x_1}^{-1,\mathrm{m}},\overline{x_2}^{-1,\mathrm{m}})$ coincides with the fixed point $\overline{\mathbf{x}}_{\mathrm{mm}}$ (see Theorems 4.1, 4.2). One thus obtains three pre-images of $\overline{\mathbf{x}}_{\mathrm{mm}}$ in $\tilde{\Omega}_{ll}$, $\tilde{\Omega}_{l\mathrm{m}}$, $\tilde{\Omega}_{\mathrm{m}l}$, as the construction is restricted to the left-hand part of f_h. Similar construction can be performed for the right-hand part of f_h.

For further pre-images of $\overline{\mathbf{x}}_{\mathrm{mm}}$, we consider the following equations:

$$\alpha x_1+\omega g_\rho(x_1)+\omega_{12}g_0(x_2)=\overline{x_1}^{-1,*},$$

$$\alpha x_2+\omega g_\rho(x_2)+\omega_{21}g_0(x_1)=\overline{x_2}^{-1,\star},$$

where ''$*$'',''$\star$''$\in\{l,\mathrm{m}\}$ if the left-hand part of f_h is considered and ''$*$'',''$\star$''$\in\{\mathrm{r},\mathrm{m}\}$ if the right-hand part of f_h is considered. Figure 3 presents such a scenario on the plane. Fixed point $\overline{\mathbf{x}}_{\mathrm{mm}}$ in the middle region has a first pre-image in region $\tilde{\Omega}_{\mathrm{m}l}$, $\tilde{\Omega}_{ll}$, and $\tilde{\Omega}_{l\mathrm{m}}$. Each of these pre-images can have their further pre-images back in $\tilde{\Omega}_{\mathrm{mm}}$. In Sec. III, (PC-1-c) and (PC-2-c) involving assumptions on the upper map $\hat{f}$ and the lower map $\check{f}$ give sufficient conditions for this scenario to take place.

In order to have these pre-images tend back toward $\overline{\mathbf{x}}_{\mathrm{mm}}$, a compactness property on the regions is needed. Thus, we further restrict these constructions to subregions Ω_{**} of $\tilde{\Omega}_{**}$. Precise confirmations for constructing these first pre-

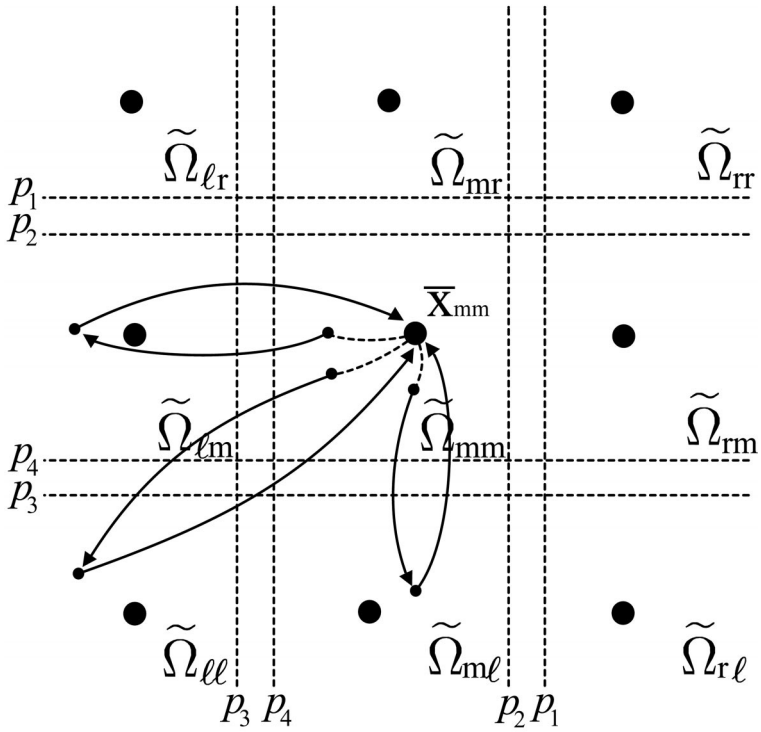

FIG. 3. The middle big dot denotes the snap-back repeller $\overline{\mathbf{x}}_{mm}$ of F in Ω_{mm}. The other small dots are successive pre-images of $\overline{\mathbf{x}}_{mm}$ under F. The graph shows that there exist three homoclinic orbits for $\overline{\mathbf{x}}_{mm}$ in the case (PC-1-a,-b,-c(i)).

images of fixed point and further pre-images are all implemented through Brouwer's fixed point theorem again (Theorems 4.1 and 4.2).

III. BASIC LEMMAS AND THE ONE-DIMENSIONAL TCNN

To study the multidimensional map (1.4), we elaborate on an analogue of the single neuron map. For fixed parameters $\varepsilon \neq 0$ and $\alpha, \omega, \rho, k \in \mathbb{R}$, we consider the following one-dimensional map:

$$f(x) = \alpha x + \omega g_\rho(x) + k, \tag{3.1}$$

$$g_\rho(x) := (1 + e^{-x/\varepsilon})^{-1} - \rho. \tag{3.2}$$

Note that $g_\rho(x)$ is a vertical shift of $g_0(x) = (1 + e^{-x/\varepsilon})^{-1}$, the output function in (1.2). The role of ρ is as a_{0i} in (1.1) and (1.4). The range of ρ in observing interesting chaotic phenomena is $0 < \rho < 1$, as the consideration in Refs. 7 and 8. We thus confine ourselves to $0 < \rho < 1$. Throughout this presentation, we consider $k \geq 0$ and discuss mainly the case $\varepsilon > 0$. To investigate the parameters which give rise to snap-back repellers for f in (3.1), we locate the points $p_1, p_2, p_3,$ and p_4 such that $f'(p_1) = f'(p_3) = -1 - (k/4\varepsilon)$ and $f'(p_2) = f'(p_4) = 1 + (k/4\varepsilon)$. It can be computed that, $p_1 = \varepsilon L_+(\varepsilon(1 + \alpha + (k/4\varepsilon)))$, $p_2 = \varepsilon L_+(\varepsilon(-1 + \alpha - (k/4\varepsilon)))$, $p_3 = \varepsilon L_-(\varepsilon(1 + \alpha + (k/4\varepsilon)))$, and $p_4 = \varepsilon L_-(\varepsilon(-1 + \alpha - (k/4\varepsilon)))$. Herein, for a fixed parameter ω, the functions L_+, L_- are defined as

$$L_+(\eta) := \mathrm{Log} \frac{2\eta}{-2\eta - \omega + \sqrt{\omega}\sqrt{4\eta + \omega}}, \tag{3.3}$$

$$L_-(\eta) := \mathrm{Log} \frac{2\eta}{-2\eta - \omega - \sqrt{\omega}\sqrt{4\eta + \omega}}. \tag{3.4}$$

Lemma A.1 in Appendix A describes several basic properties for the functions L_+, L_-. The motivation for locating these points at which the slopes of f are $1 + (k/4\varepsilon)$ and $-1 - (k/4\varepsilon)$ is to get control on the eigenvalues for the derivative of the multidimensional map (1.4) in certain regions of the phase space, as to be seen in Sec. IV. Herein, to save notations, in (3.3), (3.4), we take $\sqrt{\omega}\sqrt{4\eta + \omega} = (i\sqrt{|\omega|}) \times (i\sqrt{|4\eta + \omega|}) = -\sqrt{|\omega|}\sqrt{|4\eta + \omega|}$, as $\omega < 0$ and $4\eta + \omega < 0$.

In this presentation, we consider four groups of parameter conditions (PC) for the parameters $(\varepsilon, \alpha, \omega, \rho, k)$. They are labeled by (PC-1), (PC-2), (PC-3), and (PC-4). Each (PC-j) contains up to three subconditions (PC-j-a), (PC-j-b), (PC-j-c). There are several versions for (PC-j-c), as to be described later. For simplicity, we focus our discussions mainly on the conditions (PC-1) and (PC-2). Let us describe these conditions successively,

$$\text{(PC-1-a)} \quad \varepsilon > 0, \ \varepsilon\left(1 + \alpha + \frac{k}{4\varepsilon}\right) < 0, \quad \omega > 0,$$

$$4\varepsilon\left(-1 + \alpha - \frac{k}{4\varepsilon}\right) + \omega > 0.$$

$$\text{(PC-2-a)} \quad \varepsilon > 0, \ \varepsilon\left(-1 + \alpha - \frac{k}{4\varepsilon}\right) > 0, \quad \omega < 0,$$

$$4\varepsilon\left(1 + \alpha + \frac{k}{4\varepsilon}\right) + \omega < 0.$$

Notably, with $\varepsilon, k \geq 0$, (PC-1-a) implies $\alpha < -1$ and (PC-2-a) implies $\alpha > 1$. Under (PC-1-a) or (PC-2-a), $p_1, p_2, p_3,$ and p_4 are well defined. It follows from Lemma A.1 that the order among p_1, p_2, p_3, p_4 can be determined. Moreover,

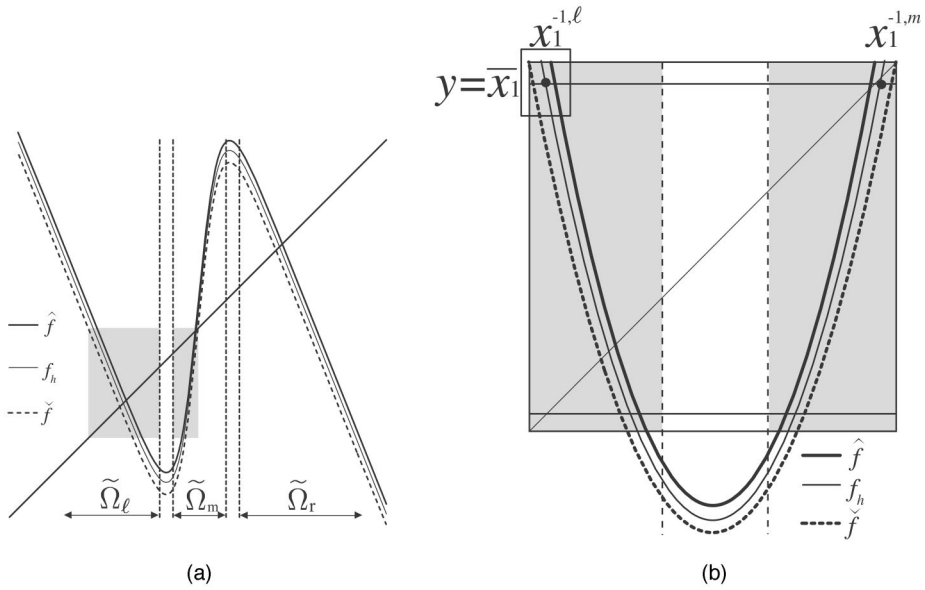

FIG. 4. Configuration for $\hat{f},f_h,\check{f}$ under the condition (PC-1-a,-b,-c(i)). (a) Configuration for $\hat{f},f_h,\check{f}$. (b) Blow-up of the shaded area of (a), $\overline{x_1}\in\widetilde{\Omega}_m$ is the first coordinate of a fixed point. $x_1^{-1,l}$ and $x_1^{-1,m}$ are two pre-images of $\overline{x_1}$ under f_h, lying in $\widetilde{\Omega}_l,\widetilde{\Omega}_m$, respectively.

the slopes of f on the intervals partitioned by p_1,p_2,p_3,p_4 can be estimated. The proof of the following lemma is given in Appendix A.

Lemma 3.1. (i) If (PC-1-a) holds, then $p_1>p_2>p_4>p_3$. In addition, $f'(x)>1+(k/4\varepsilon)$ for $p_4<x<p_2$ and $f'(x)<-1-(k/4\varepsilon)$ for $x>p_1$ or $x<p_3$. (ii) If (PC-2-a) holds, then $p_2>p_1>p_3>p_4$. In addition, $f'(x)<-1-(k/4\varepsilon)$ for $p_3<x<p_1$ and $f'(x)>1+(k/4\varepsilon)$ for $x>p_2$ or $x<p_4$.

Set, for conditions (PC-1) and (PC-2), respectively,

$$\widetilde{\Omega}^l:=\{x\in\mathbb{R}|x\leqslant p_3\},\quad \widetilde{\Omega}^m:=\{x\in\mathbb{R}|p_4\leqslant x\leqslant p_2\},$$

$$\widetilde{\Omega}^r:=\{x\in\mathbb{R}|x\geqslant p_1\},\tag{3.5}$$

$$\widetilde{\Omega}^l:=\{x\in\mathbb{R}|x\leqslant p_4\},\quad \widetilde{\Omega}^m:=\{x\in\mathbb{R}|p_3\leqslant x\leqslant p_1\},$$

$$\widetilde{\Omega}^r:=\{x\in\mathbb{R}|x\geqslant p_2\}.\tag{3.6}$$

Herein, "l," "m," and "r" mean "left-hand region," "middle region," and "right-hand region," respectively. According to the above setting, $\mathbb{R}$ is partitioned into five regions. The snap-back repellers and their homoclinic orbits for (3.1) to be constructed will be located in the three regions (3.5) or (3.6). Configuration for f satisfying (PC-1-a) and (3.5) is as illustrated in Fig. 2.

The following formulation on a family of one-dimensional maps analogous to (3.1) is prepared for the study on the multidimensional map (1.4). For fixed α, ω, $\varepsilon\neq 0$, $0<\rho<1$, and $k>0$, we consider

$$\hat{f}(x)=\alpha x+\omega g_\rho(x)+k,\tag{3.7}$$

$$\check{f}(x)=\alpha x+\omega g_\rho(x)-k,\tag{3.8}$$

$$f_h(x)=\alpha x+\omega g_\rho(x)+h,\tag{3.9}$$

where $h\in\mathbb{R}$ with $-k\leqslant h\leqslant k$. It follows that $\check{f}\leqslant f_h\leqslant\hat{f}$ and $f_k=\hat{f}$, $f_{-k}=\check{f}$. Corresponding to this setting, further parameter conditions for $(\varepsilon,\alpha,\omega,\rho,k)$ are formulated as follows:

(PC-1-b) $$g_\rho(p_1)>\frac{1-\alpha}{\omega}p_1+\frac{k}{\omega},$$

$$g_\rho(p_3)<\frac{1-\alpha}{\omega}p_3-\frac{k}{\omega}.$$

(PC-2-b) $$g_\rho(p_2)>\frac{1-\alpha}{\omega}p_2-\frac{k}{\omega},$$

$$g_\rho(p_4)<\frac{1-\alpha}{\omega}p_4+\frac{k}{\omega}.$$

Each of these conditions imposes a restriction on the family of maps $\{f_h\}$. The configuration for g_ρ with the parameters $(\varepsilon,\alpha,\omega,\rho,k)$ satisfying (PC-1-b) is illustrated in Fig. 5. Notably, $\alpha\overline{x}+\omega g_\rho(\overline{x})+h=\overline{x}$ if and only if $y=g_\rho(\overline{x})$ and $y=[(1-\alpha)\overline{x}-h]/\omega$. Thus, under conditions (PC-j-a), (PC-j-

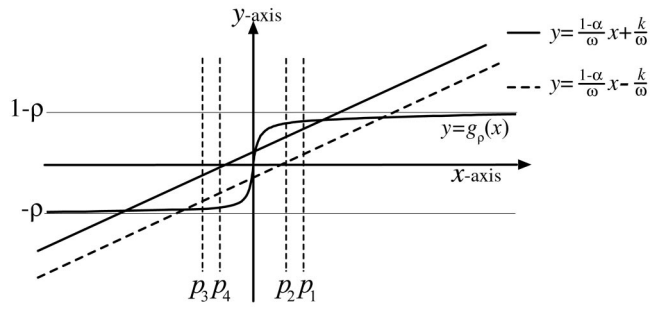

FIG. 5. (PC-1-b) means that the point $(p_1,g_\rho(p_1))$ is higher than the point $(p_1,[(1-\alpha)/\omega]p_1+(k/\omega))$; the point $(p_3,g_\rho(p_3))$ is lower than the point $(p_3,[(1-\alpha)/\omega]p_3-(k/\omega))$. (Note that $[(1-\alpha)/\omega]>0$, $\omega>0$.)

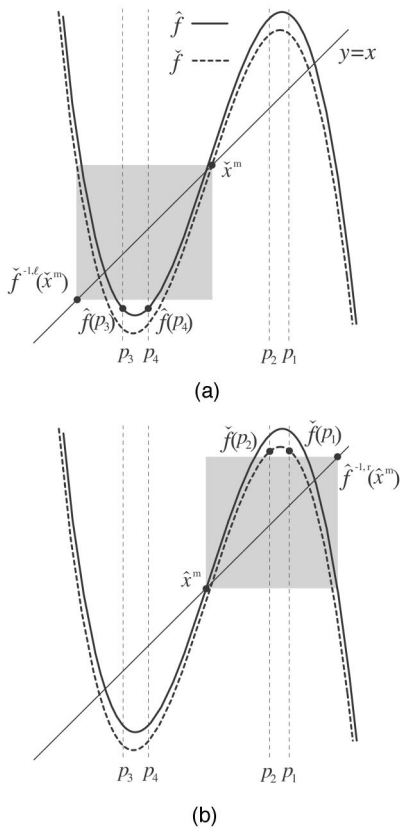

FIG. 6. (a) satisfies (PC-1-a,-b,-c(i)) with $\check{f}^{-1,l}(\check{x}^{\mathrm{m}})>\max\{\hat{f}(p_3),\hat{f}(p_4)\}$. (b) satisfies (PC-1-a,-b,-c(ii)) with $\hat{f}^{-1,\mathrm{r}}(\hat{x}^{\mathrm{m}})<\min\{\check{f}(p_1),\check{f}(p_2)\}$.

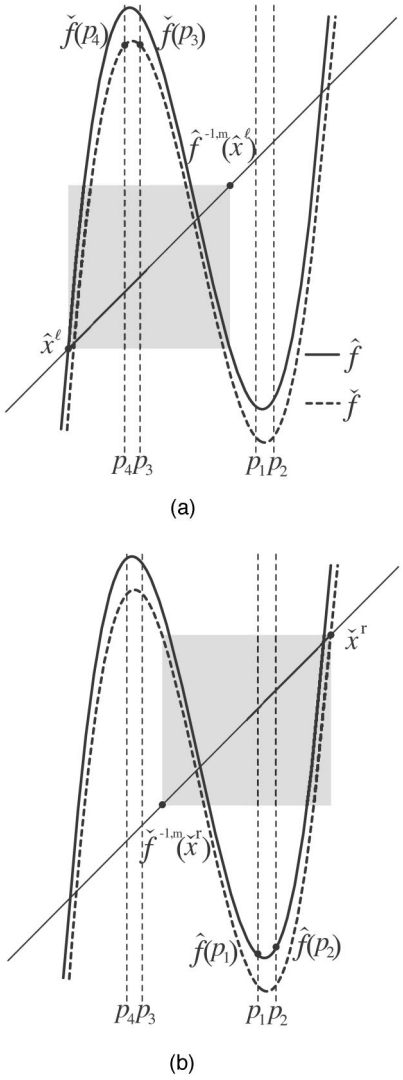

FIG. 7. (a) satisfies (PC-2-a,-b,-c(i)) with $f^{-1,\mathrm{m}}(\hat{x}^{l})<\min\{\check{f}(p_3),\check{f}(p_4)\}$. (b) satisfies (PC-2-a,-b,-c(ii)) with $\check{f}^{-1,\mathrm{m}}(\check{x}^{\mathrm{r}})>\max\{\hat{f}(p_1),\hat{f}(p_2)\}$.

b), j=1 or 2, every f_h in (3.9) has a fixed point in each of the regions $\tilde{\Omega}^{l}$, $\tilde{\Omega}^{\mathrm{m}}$, $\tilde{\Omega}^{\mathrm{r}}$. (Notably, these regions correspond to the parameters $\varepsilon,\alpha,\omega,\rho,k$.) Moreover, there are two critical points for f_h and $|f_h(x)|\to\infty$ as $|x|\to\infty$.

Let us introduce the following notations. $\hat{f}^{-1,l}(\eta),\hat{f}^{-1,\mathrm{m}}(\eta),\hat{f}^{-1,\mathrm{r}}(\eta)$ represent the pre-images of η under $\hat{f}$, which lies in $\tilde{\Omega}^{l}$, $\tilde{\Omega}^{\mathrm{m}}$, $\tilde{\Omega}^{\mathrm{r}}$, respectively. Similar notations will be used for the pre-images under $\check{f}$. $\hat{x}^{\mathrm{r}}$, $\hat{x}^{\mathrm{m}}$, $\hat{x}^{l}$ represent the fixed points of $\hat{f}$ lying in $\tilde{\Omega}^{\mathrm{r}}$, $\tilde{\Omega}^{\mathrm{m}}$, $\tilde{\Omega}^{l}$, respectively. Analogously, $\check{x}^{\mathrm{r}}$, $\check{x}^{\mathrm{m}}$, $\check{x}^{l}$ represent the fixed points of $\check{f}$ lying in the three respective regions. The following conditions guarantees that the fixed points of f_h are indeed snap-back repellers for f_h:

(PC-1-c) (i) $\check{f}^{-1,l}(\check{x}^{\mathrm{m}})>\max\{\hat{f}(p_3),\hat{f}(p_4)\}$,

(ii) $\hat{f}^{-1,\mathrm{r}}(\hat{x}^{\mathrm{m}})<\min\{\check{f}(p_1),\check{f}(p_2)\}$.

(PC-2-c) (i) $\hat{f}^{-1,\mathrm{m}}(\hat{x}^{l})<\min\{\check{f}(p_3),\check{f}(p_4)\}$,

(ii) $\check{f}^{-1,\mathrm{m}}(\check{x}^{\mathrm{r}})>\max\{\hat{f}(p_1),\hat{f}(p_2)\}$.

(iii) $\hat{f}^{-1,\mathrm{m}}(\hat{f}^{-1,l}(\check{x}^{\mathrm{m}}))<p_1$,

$\check{f}^{-1,\mathrm{m}}(\hat{f}^{-1,\mathrm{m}}(\hat{f}^{-1,l}(\check{x}^{\mathrm{m}})))>p_3$.

(iv) $\check{f}^{-1,\mathrm{m}}(\check{f}^{-1,\mathrm{r}}(\hat{x}^{\mathrm{m}}))>p_3$,

$\hat{f}^{-1,\mathrm{m}}(\check{f}^{-1,\mathrm{m}}(\check{f}^{-1,\mathrm{r}}(\hat{x}^{\mathrm{m}})))<p_1$.

Typical graphs for f_h satisfying (PC-1-a, -b, -c(i)), (PC-1-a, -b, -c(ii)), (PC-2-a, -b, -c(i)), and (PC-2-a, -b, -c(ii)) are shown in Figs. 6(a), 6(b), 7(a), and 7(b), respectively. Figure 8, while used to explain trapping regions in Sec. IV, also provides a configuration for the graphs of f_h satisfying (PC-2-a, -b, -c(iii)(iv)).

The conditions in (PC-j-c), j=1,2, involve pre-images of certain points under $\check{f}$ and $\hat{f}$. The following implications provide more straightforward conditions which can replace (PC-1-c(i)), (PC-1-c(ii)), (PC-2-c(i))–(PC-2-c(iv)), respectively. However, stronger conditions limit the feasible numerical ranges for the parameters, concerning the behaviors of TCNN we are investigating.

Lemma 3.2. Assume that (PC-1-a, -b) hold for the following items (1)–(2), and (PC-2-a, -b) hold for the following items (3)–(6). Then

(1) $\check{f}(\hat{f}(p_3))>p_2$ and $\check{f}(\hat{f}(p_4))>p_2$ imply (PC-1-c(i)),

(2) $\hat{f}(\check{f}(p_1))<p_4$ and $\hat{f}(\check{f}(p_2))<p_4$ imply (PC-1-c(ii)),

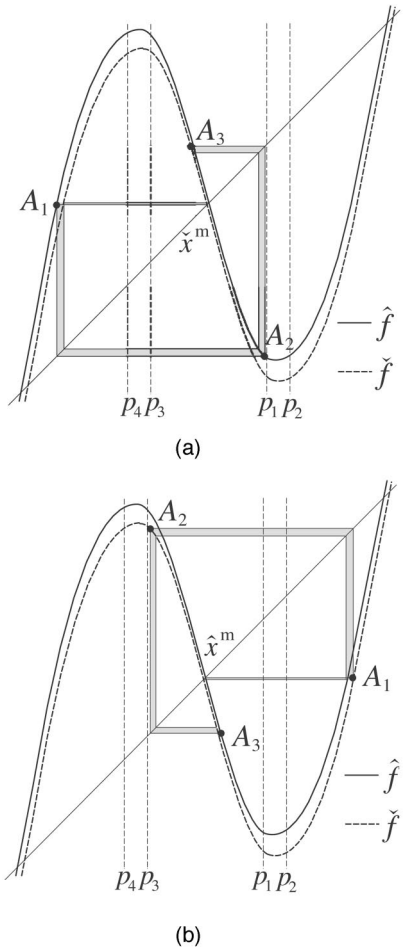

FIG. 8. (a) satisfies (PC-2-a,-b,-c(iii)). The first coordinates of points A_1, A_2, and A_3 are $\hat{f}^{-1,l}(\check{x}^{\mathrm{m}})$, $\hat{f}^{-1,\mathrm{m}}(\hat{f}^{-1,l}(\check{x}^{\mathrm{m}}))$ and $\check{f}^{-1,\mathrm{m}}(\hat{f}^{-1,\mathrm{m}}(\hat{f}^{-1,l}(\check{x}^{\mathrm{m}})))$, respectively. (b) satisfies (PC-2-a,-b,-c(iv)). The first coordinates of points A_1, A_2, and A_3 are $\check{f}^{-1,\mathrm{r}}(\hat{x}^{\mathrm{m}})$, $\check{f}^{-1,\mathrm{m}}(\check{f}^{-1,\mathrm{r}}(\hat{x}^{\mathrm{m}}))$, and $\hat{f}^{-1,\mathrm{m}}(\check{f}^{-1,\mathrm{m}}(\check{f}^{-1,\mathrm{r}}(\hat{x}^{\mathrm{m}})))$, respectively.

(3) $g_\rho(\hat{f}(p_1))>(1-\alpha)/\omega\,(\hat{f}(p_1))-(k/\omega)$, $\hat{f}(p_1)<p_3$, and $\min\{\check{f}(p_3),\check{f}(p_4)\}>p_1$ imply (PC-2-c(i)),

(4) $g_\rho(\check{f}(p_3))<(1-\alpha)/\omega\,(\check{f}(p_3))+(k/\omega)$, $p_1>\check{f}(p_3)$, and $\max\{\hat{f}(p_1),\hat{f}(p_2)\}<p_3$ imply (PC-2-c(ii)),

(5) $p_3>\hat{f}(\hat{f}(p_1))$, $\check{f}(p_3)>p_1$, and $\hat{f}(p_1)<p_4$ imply (PC-2-c(iii)),

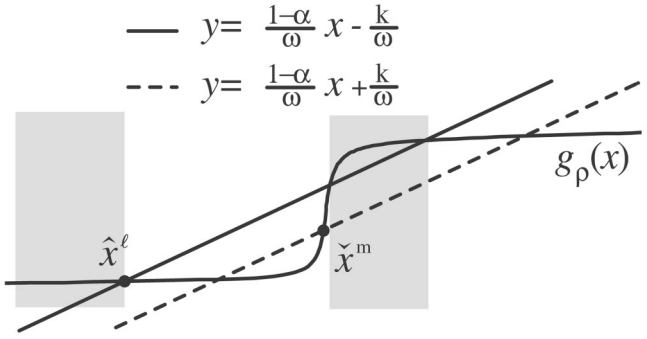

FIG. 9. $\hat{f}(p_1)$ belongs to the left shaded region. (Note that $[(1-\alpha)/\omega]>0$, $\omega<0$.)

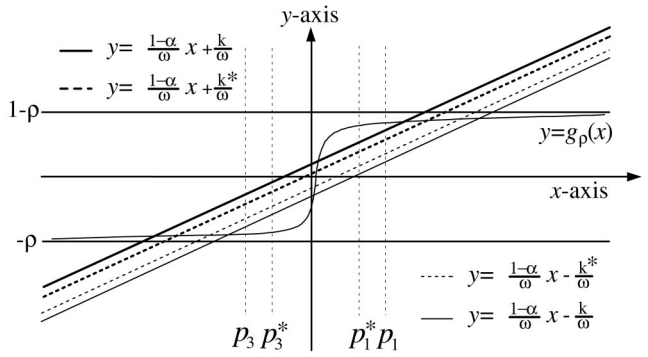

FIG. 10. Illustration for the condition (PC-1) in Remark 3.3. p_j^* corresponds to the case with parameter k^*.

(6) $p_1<\check{f}(\check{f}(p_3))$, $\hat{f}(p_1)<p_3$ and $\check{f}(p_3)>p_2$ imply (PC-2-c(iv)).

Proof. The basic idea of the lemma is to compare the values of $\hat{f}$ and $\check{f}$ at various related points. Figure 6(a) demonstrates the situation of case (1). $\check{f}(\hat{f}(p_3))>\check{x}^{\mathrm{m}}$ follows from $p_2>\check{x}^{\mathrm{m}}$ and $\check{f}(\hat{f}(p_3))>p_2$. $\hat{f}(p_3)<p_3$ yields $\hat{f}(p_3)\in\tilde{\Omega}^l$. Accordingly, $\check{f}^{-1,l}(\check{f}(\hat{f}(p_3)))<\check{f}^{-1,l}(\check{x}^{\mathrm{m}})$, since $\check{f}$ is decreasing on $\tilde{\Omega}^l$. Thus, $\hat{f}(p_3)<\check{f}^{-1,l}(\check{x}^{\mathrm{m}})$. Same arguments apply to the condition $\hat{f}(p_4)<\check{f}^{-1,l}(\check{x}^{\mathrm{m}})$. This justifies case (1).

For case (3), we shall show that (PC-2-c(i)) holds. It follows from $g_\rho(\hat{f}(p_1))>[(1-\alpha)/\omega](\hat{f}(p_1))-(k/\omega)$ that $\hat{f}(p_1)$ may belong to the left shaded region or the right shaded region of Fig. 9. With $\hat{f}(p_1)<p_3$ and $p_3<\check{x}^{\mathrm{m}}$ implying $\hat{f}(p_1)<\check{x}^{\mathrm{m}}$, it is confirmed that $\hat{f}(p_1)$ belongs to the left shaded region. Note that $p_1>\hat{f}^{-1,\mathrm{m}}(\hat{x}^l)$ since $\hat{f}(p_1)<\hat{x}^l$. With the assumption $\min\{\check{f}(p_3),\check{f}(p_4)\}>p_1$, we have $\min\{\check{f}(p_3),\check{f}(p_4)\}>\hat{f}^{-1,\mathrm{m}}(\hat{x}^l)$. This completes the proof for case (3). We omit the proofs for other cases since they are similar.

Remark 3.3. It can be observed that if $(\varepsilon,\alpha,\omega,\rho,k)$ satisfies any of the above conditions, (PC-j-a), (PC-j-b), (PC-j-c(i))-(PC-j-c(iv)), j=1, 2, then for $0\leqslant k^*<k$, $(\varepsilon,\alpha,\omega,\rho,k^*)$ also satisfies these conditions. Figures 10 and 11 demonstrate this observation.

The following proposition concludes the existence of fixed points and snap-back repellers for the family of one-dimensional maps $\{f_h\}$. Its proof is given in Appendix A.

Proposition 3.4. Assume that $k>0$ and the parameters $(\varepsilon,\alpha,\omega,\rho,k)$ satisfy (PC-1-a, -b) [respectively, (PC-2-a, -b)]. Let the regions $\tilde{\Omega}^{\mathrm{r}},\tilde{\Omega}^{\mathrm{m}},\tilde{\Omega}^l$ be as defined in (3.5) [respectively, (3.6)] according to the parameters $(\varepsilon,\alpha,\omega,\rho,k)$. Then for every h with $-k\leqslant h\leqslant k$, the following assertions hold.

(i) There exist three fixed points $\overline{x}_h^{\mathrm{r}}\in\tilde{\Omega}^{\mathrm{r}}$, $\overline{x}_h^{\mathrm{m}}\in\tilde{\Omega}^{\mathrm{m}}$ and $\overline{x}_h^{l}\in\tilde{\Omega}^{l}$, for the map f_h.

(ii) If the parameters $(\varepsilon,\alpha,\omega,\rho,k)$ further satisfy (PC-1-c(i)) [respectively (PC-2-c(i))], then $\overline{x}_h^{l}$ and $\overline{x}_h^{\mathrm{m}}$ are snap-back repellers.

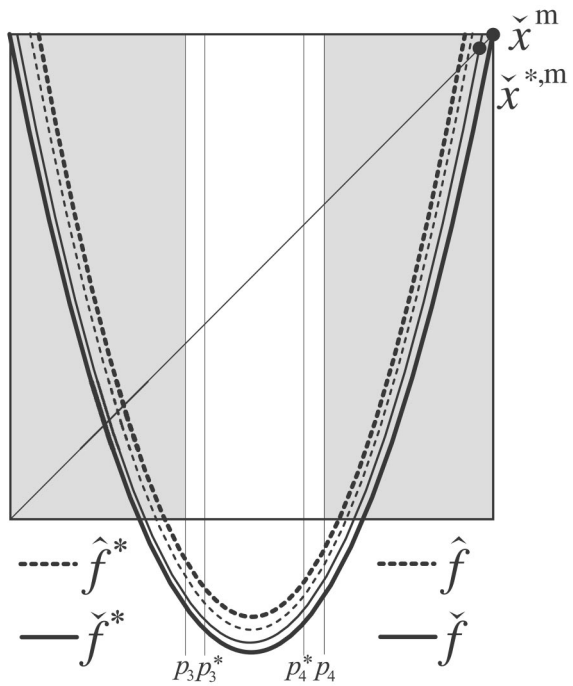

FIG. 11. Illustration for the condition (PC-1-c(i)) in Remark 3.3. p_j^*, $\check{f}^*$, $\hat{f}^*$, $\check{x}^{*,m}$ correspond to the situation with parameter k^*.

(iii) If the parameters $(\varepsilon,\alpha,\omega,\rho,k)$ further satisfy (PC-1-c(ii)) [respectively (PC-2-c(ii))], then $\overline{x}_h^{m}$ and $\overline{x}_h^{r}$ are snap-back repellers.

(iv) If the parameters $(\varepsilon,\alpha,\omega,\rho,k)$ further satisfy (PC-2-c(iii)) or (PC-2-c(iv)), then $\overline{x}_h^{m}$ is a snap-back repeller.

In fact, our formulations also provide the following indications. Recall the previous notations $\hat{x}^{r}$, $\hat{x}^{m}$, $\hat{x}^{l}$, $\check{x}^{r}$, $\check{x}^{m}$, $\check{x}^{l}$. In addition, $\hat{f}^{-1,r}(\hat{x}^{m})$ [respectively, $\check{f}^{-1,l}(\check{x}^{m})$] means the pre-image of $\hat{x}^{m}$ (respectively, $\check{x}^{m}$) under $\hat{f}$ (respectively, $\check{f}$), which lies on Ω^{r} (respectively, Ω^{l}).

Proposition 3.5. Let h with $-k\leqslant h\leqslant k$ be fixed.

(i) Assume that (PC-1-a, -b, -c(i)) [respectively, (PC-2-a, -b, -c(i))] hold. For every $\varsigma\in[\check{f}^{-1,l}(\check{x}^{m}),\check{x}^{m}]$ (respectively, $[\hat{x}^{l},\hat{f}^{-1,m}(\hat{x}^{l})]$), there exist two points $\xi'\in\tilde{\Omega}^{l}$ and $\xi''\in\tilde{\Omega}^{m}$ such that $f_h(\xi')=f_h(\xi'')=\varsigma$.

(ii) Assume that (PC-1-a, -b, -c(ii)) [respectively, (PC-2-a, -b, -c(ii))] hold. Then for every $\varsigma\in[\hat{x}^{m},\hat{f}^{-1,r}(\hat{x}^{m})]$ (respectively, $[\check{f}^{-1,m}(\check{x}^{r}),\check{x}^{r}]$), there exist two points $\xi'\in\tilde{\Omega}^{r}$ and $\xi''\in\tilde{\Omega}^{m}$ such that $f_h(\xi')=f_h(\xi'')=\varsigma$.

We use Fig. 12(a) to illustrate case (ii) of this proposition. Similar results can be derived for (PC-2-a, -b, -c(iii), -c(iv)), as demonstrated in Fig. 12(b). Proposition 3.5 will be used to construct pre-images of the fixed points for the multidimensional maps in the next section. As for an intuitive sense on the parameters in Proposition 3.4, we have the following observation. In general, with fixed ε, α, ω, ρ, the smaller k the more likely that the parameter conditions (PC-j) can be satisfied. Furthermore, if the parameters $\varepsilon,\alpha,\omega,0<\rho<1$ and $k=0$ satisfy (PC-1-a) or (PC-2-a), then

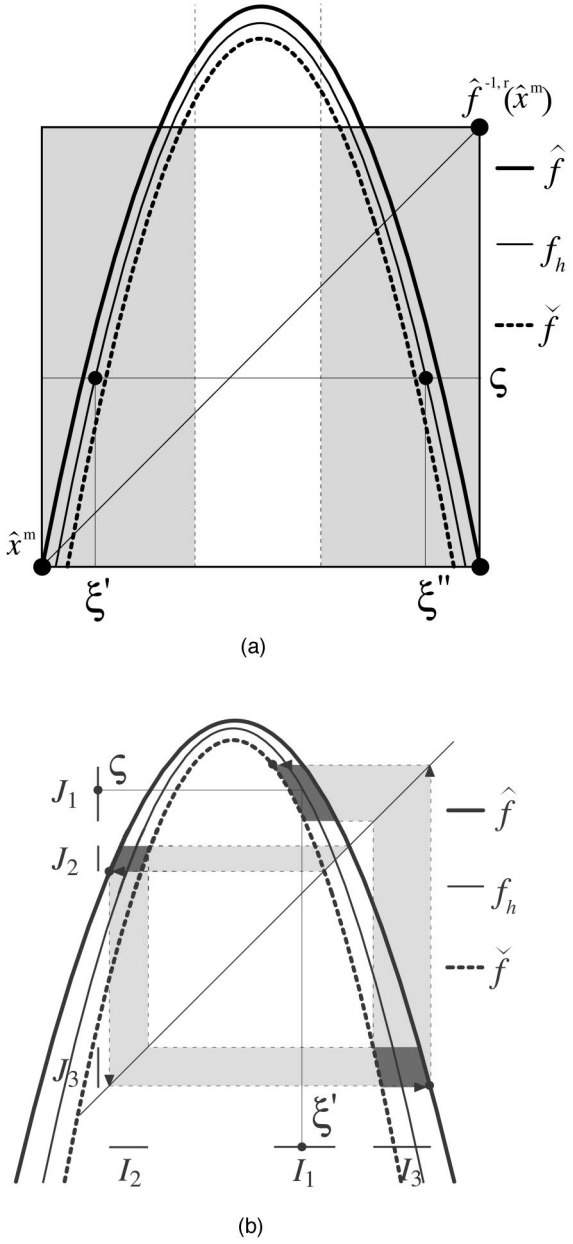

FIG. 12. Illustrations for Proposition 3.5. (a) $f_h(\xi')=f_h(\xi'')=\varsigma$, where ξ' (respectively, ξ'') belongs to the left (respectively, right) shaded region. This figure explains the conditions (PC-1-c(ii)). (b) If $\varsigma\in J_j$ then there is $\xi'\in I_i$, such that $f_h(\xi')=\varsigma$, $j=1,2,3$. This figure explains the conditions (PC-2-c(iii)(iv)).

the scenarios in Proposition 3.4 also hold for sufficiently small k. On the other hand, if $(\varepsilon,\alpha,\omega,\rho,k)$ satisfies the condition of Proposition 3.4, so does $(\varepsilon,\alpha,\omega,\rho,k^*)$ for each k^* with $0\leqslant k^*<k$, as seen in Remark 3.3. This observation indicates that chaotic behaviors take place under the situation of a fixed nonzero self-feedback connection weight ω versus small connection weights between distinct neurons, which are dominated by k (see Sec. IV). This observation can be compared to the conditions in Refs. 7 and 8, which takes ω to infinity, while holding k fixed. More than this comparison, our methodology actually provides explicit parameter ranges for chaos on a large scale. The numerical ranges for the parameters satisfying these conditions (PC) will be illustrated in Sec. VI.

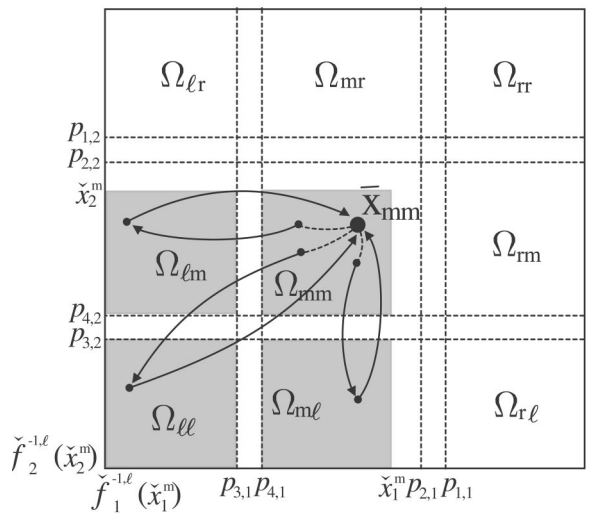

FIG. 13. Illustrations for the regions $\Omega_{*,\star}$, "*," "$\star$" $\in\{r,m,l\}$. Successive preimages of $\overline{\mathbf{x}}_{mm}$ under F are demonstrated in the shaded area, under condition (PC-1-a,-b,-c(i)).

For each h with $-k\leqslant h\leqslant k$, we shall construct the homoclinic orbits of f_h in the following subregions $\Omega^l,\Omega^m,\Omega^r$ of $\tilde{\Omega}^l,\tilde{\Omega}^m,\tilde{\Omega}^r$, respectively, where, for condition (PC-1) and (PC-2), respectively,

$$\Omega^l:=\tilde{\Omega}^l\cap[\check{f}^{-1,l}(\check{x}^m),\check{x}^m],$$

$$\Omega^m:=\tilde{\Omega}^m,\quad \Omega^r:=\tilde{\Omega}^r\cap[\hat{x}^m,\hat{f}^{-1,r}(\hat{x}^m)], \tag{3.10}$$

$$\Omega^l:=\tilde{\Omega}^l\cap[\hat{x}^l,\hat{f}^{-1,m}(\hat{x}^l)],$$

$$\Omega^m:=\tilde{\Omega}^m,\quad \Omega^r:=\tilde{\Omega}^r\cap[\check{f}^{-1,m}(\check{x}^r),\check{x}^r]. \tag{3.11}$$

Figure 13 is an illustration of these regions in the phase space of dimension two, that is, $n=2$, the two-neuron case. For (PC-2-c(iii)(iv)), (3.10), (3.11) should be adjusted to

$$\Omega^l:=\{x|\check{x}^l\leqslant x\leqslant p_4\},$$

$$\Omega^m:=\{x|p_3\leqslant x\leqslant p_1\},$$

$$\Omega^r:=\{x|p_2\leqslant x\leqslant\hat{x}^r\}.$$

The compactness of these regions will be used to assure the convergence of pre-images for fixed points in the next section. Notably, the fixed points $\overline{x}_h^r$, $\overline{x}_h^m$, $\overline{x}_h^l$ in Proposition 3.4 (i) lie in Ω^r, Ω^m, Ω^l, respectively; the assertions in Proposition 3.5 also hold for ς in smaller ranges Ω^l or Ω^r.

The previous results also hold for $\varepsilon<0$. The following two groups of conditions yield parallel results to the ones in Lemmas 3.1, 3.2, Propositions 3.4 and 3.5,

(PC-3-a) $\varepsilon<0,\ \varepsilon\left(-1+\alpha-\dfrac{k}{4|\varepsilon|}\right)<0,\ \omega>0,$

$$4\varepsilon\left(1+\alpha+\frac{k}{4|\varepsilon|}\right)+\omega>0,$$

(PC-3-b) $g_\rho(p_4)>\dfrac{1-\alpha}{\omega}p_4+\dfrac{k}{\omega},$

$$g_\rho(p_2)<\frac{1-\alpha}{\omega}p_2-\frac{k}{\omega},$$

(PC-3-c) (i) $\hat{f}^{-1,m}(\hat{x}^l)<\min\{\check{f}(p_1),\check{f}(p_2)\}$,

(ii) $\check{f}^{-1,m}(\check{x}^r)>\max\{\hat{f}(p_3),\hat{f}(p_4)\}$,

(iii) $\hat{f}^{-1,m}(\hat{f}^{-1,l}(\check{x}^m))<p_3$,

$\check{f}^{-1,m}(\hat{f}^{-1,m}(\hat{f}^{-1,l}(\check{x}^m)))>p_1$,

(iv) $\check{f}^{-1,m}(\check{f}^{-1,r}(\hat{x}^m))>p_1$,

$\hat{f}^{-1,m}(\check{f}^{-1,m}(\check{f}^{-1,r}(\hat{x}^m)))<p_3$,

(PC-4-a) $\varepsilon<0,\ \varepsilon\left(1+\alpha+\dfrac{k}{4|\varepsilon|}\right)>0,$

$$\omega<0,\ 4\varepsilon\left(-1+\alpha-\frac{k}{4|\varepsilon|}\right)+\omega<0,$$

(PC-4-b) $g_\rho(p_3)>\dfrac{1-\alpha}{\omega}p_3-\dfrac{k}{\omega},\ g_\rho(p_1)<\dfrac{1-\alpha}{\omega}p_1+\dfrac{k}{\omega},$

(PC-4-c) (i) $\check{f}^{-1,l}(\check{x}^m)>\max\{\hat{f}(p_1),\hat{f}(p_2)\}$,

(ii) $\hat{f}^{-1,r}(\hat{x}^m)<\min\{\check{f}(p_3),\check{f}(p_4)\}$,

where $p_1=\varepsilon L_+(\varepsilon(1+\alpha+(k/4|\varepsilon|)))$, $p_2=\varepsilon L_+(\varepsilon(-1+\alpha-(k/4|\varepsilon|)))$, $p_3=\varepsilon L_-(\varepsilon(1+\alpha+(k/4|\varepsilon|)))$, $p_4=\varepsilon L_-(\varepsilon(-1+\alpha-(k/4|\varepsilon|)))$.

IV. SNAP-BACK REPELLERS FOR TCNN

We aim to study the existence of snap-back repellers for the multidimensional TCNN (1.2), (1.4) in this section. For convenience of discussion, we set $\omega_{ii}=\omega$ for each i. Recalling g_ρ in (3.2), we rewrite (1.4) as the following n-dimensional map: $F:\mathbb{R}^n\to\mathbb{R}^n$ with $F=(F_1,\ldots,F_n)$, where

$$F_i(\mathbf{x})=\alpha x_i+\omega g_{\rho_i}(x_i)+\Sigma_{j=1,j\neq i}^n\omega_{ij}g_0(x_j)+a_i, \tag{4.1}$$

$\mathbf{x}=(x_1,\ldots,x_n)$, and $\rho_i:=a_{0i}$ is restricted to the interval (0, 1). We propose the following upper and lower one-dimensional maps for each component F_i. Let

$$\hat{f}_i(x)=\alpha x+\omega g_{\rho_i}(x)+k_i,$$

$$\check{f}_i(x)=\alpha x+\omega g_{\rho_i}(x)-k_i,$$

where $x\in\mathbb{R}$ and k_i is a number greater than $\Sigma_{j=1,j\neq i}^n(|\omega_{ij}|+|a_i|)$. Notably, for each i, $-\rho_i<g_{\rho_i}(x_i)<1-\rho_i$ and $0<g_0(x_i)<1$ for all $x_i\in\mathbb{R}$. Following the formulations in Sec. III, we obtain $p_{1,i},p_{2,i},p_{3,i},p_{4,i}$ for each i and accordingly, the regions $\Omega_i^l,\Omega_i^m,\Omega_i^r$, as defined in (3.10) and (3.11). Consequently, we focus on the map (4.1) in the following 3^n regions:

$$\Omega_{j_1\cdots j_n}:=\{(x_1,\ldots,x_n)\in\mathbb{R}^n|x_1\in\Omega_1^{j_1},\ldots,x_n\in\Omega_n^{j_n}\},$$

where $j_i=$ "l" or "m" or "r."

Theorem 4.1. If each $k_i>0$ and each $(\varepsilon,\alpha,\omega,\rho_i,k_i)$, $i=1,\ldots,n$, satisfies (PC-1-a, -b) or (PC-2-a, -b), then the system (4.1) has 3^n fixed points.

Proof. It follows from the assumption of the theorem that every component $F_i(\mathbf{x})$ of the map $F(\mathbf{x})$ satisfies

$$\check{f}_i(x_i)\leqslant F_i(\mathbf{x})\leqslant\hat{f}_i(x_i). \tag{4.2}$$

Consider a fixed $\Omega_{j_1\cdots j_n}$ for certain $j_i=$''l'' or ''m'' or ''r.'' Let $(\xi_1',\ldots,\xi_n')\in\Omega_{j_1\cdots j_n}$. Then, by Proposition 3.4 (i), there exist $\xi_i^l\in\Omega_i^l$, $\xi_i^{\mathrm{m}}\in\Omega_i^{\mathrm{m}}$, $\xi_i^{\mathrm{r}}\in\Omega_i^{\mathrm{r}}$, such that

$$\xi_i^*=\alpha\xi_i^*+\omega g_{\rho_i}(\xi_i^*)+\sum_{j=1,j\neq i}^{n}\omega_{ij}g_0(\xi_j')+a_i, \tag{4.3}$$

where ''$*$''=''l,'' ''m,'' ''r.'' Restated, each ξ_i^* is a fixed point of the one-dimensional map $\xi_i\mapsto\alpha\xi_i+\omega g_{\rho_i}(\xi_i)+\Sigma_{j=1,j\neq i}^{n}\omega_{ij}g_0(\xi_j')+a_i$. Let $H:\Omega_{j_1\cdots j_n}\to\Omega_{j_1\cdots j_n}$ be defined by $H(\xi_1',\ldots,\xi_n')=(\xi_1^{j_1},\ldots,\xi_n^{j_n})$. We want to show that there exists a fixed point for H. Define $G:\mathbb{R}^n\times\mathbb{R}^n\to\mathbb{R}^n$ by

$$G_i(\mathbf{x}',\mathbf{x})=x_i-\alpha x_i-\omega g_{\rho_i}(x_i)-\sum_{j=1,j\neq i}^{n}\omega_{ij}g_0(x_j')-a_i,$$

where $i=1,\ldots,n$. Notably, $G(\mathbf{x}',H(\mathbf{x}'))=0$ for every $\mathbf{x}'\in\Omega_{j_1\cdots j_n}$, by (4.3). Now,

$$\frac{\partial G}{\partial\mathbf{x}}(\mathbf{x}',\mathbf{x})=\mathrm{diag}[\chi_1,\ldots,\chi_n]$$

$$:=\begin{pmatrix}\chi_1 & 0 & \cdots & 0 & 0\\ 0 & \chi_2 & \ddots & 0 & 0\\ \vdots & \ddots & \ddots & \ddots & \vdots\\ 0 & 0 & \ddots & \chi_{n-1} & 0\\ 0 & 0 & \cdots & 0 & \chi_n\end{pmatrix}, \tag{4.4}$$

where $\chi_i=1-\alpha-\omega g_{\rho_i}'(x_i)$, $i=1,\ldots,n$. For $\mathbf{x}=(x_1,\ldots,x_n)\in\Omega_{j_1\cdots j_n}$, we have $|\alpha+\omega g_{\rho_i}'(x_i)|\geq 1+(k_i/4\varepsilon)$ for each i, according to Lemma 3.1. It follows that H is a C^1 function, by the implicit function theorem. Hence, by the Brouwer fixed point theorem, there exists one fixed point $\overline{\mathbf{x}}$ of H in $\Omega_{j_1\cdots j_n}$, which is also a fixed point of F. In fact, there exists only one fixed point in each $\Omega_{j_1\cdots j_n}$, as to be seen in the proof of Theorem 4.2. Consequently, there are 3^n fixed points of F in $\mathbb{R}^n$.

Theorem 4.2. Assume that each $k_i>0$ and each $(\varepsilon,\alpha,\omega,\rho_i,k_i)$, $i=1,\ldots,n$, satisfies (PC-1-a), (PC-1-b) [respectively (PC-2-a), (PC-2-b)].

(i) If each $(\varepsilon,\alpha,\omega,\rho_i,k_i)$ further satisfies (PC-1-c(i)) or (PC-1-c(ii)) [respectively (PC-2-c(i)) or (PC-2-c(ii))], then system (4.1) has at least 2^n snap-back repellers.

(ii) If each $(\varepsilon,\alpha,\omega,\rho_i,k_i)$ further satisfies (PC-1-c(i)) and (PC-1-c(ii)) [respectively (PC-2-c(i)) and (PC-2-c(ii))], then system (4.1) has 3^n snap-back repellers.

(iii) If each $(\varepsilon,\alpha,\omega,\rho_i,k_i)$ satisfies (PC-2-a), (PC-2-b), and (PC-2-c(iii)) or (PC-2-c(iv)), then system (4.1) has at least one snap-back repeller in the middle region $\Omega_{\mathrm{m}\cdots\mathrm{m}}$.

Proof. The idea of the proof is to construct pre-images of fixed points via the Brouwer fixed point theorem. We shall only prove the (PC-1) case. The proofs for the other cases are similar. Notably, (PC-1-a) and (PC-1-b) imply the existence of 3^n fixed points of (4.1), due to Theorem 4.1. Each of the 3^n regions $\Omega_{j_1\cdots j_n}$, $j_i=$''l'' or ''m'' or ''r'' contains exactly one of these fixed points. The proof is divided into three steps (I), (II), and (III).

(I) Recall the notations in Proposition 3.5. Assume that (PC-1-a), (PC-1-b), and (PC-1-c(i)) hold. Let $x_i\in\Omega_i^l$. By Proposition 3.5 and Eq. (4.2), for each $\xi_i'\in\Omega_i^{\mathrm{m}}$ (respectively, Ω_i^l), there exists $\xi_i\in\Omega_i^{\mathrm{m}}$ (respectively, Ω_i^l) such that

$$x_i=\alpha\xi_i+\omega g_{\rho_i}(\xi_i)+\sum_{j=1,j\neq i}^{n}\omega_{ij}g_0(\xi_j')+a_i. \tag{4.5}$$

Similarly, for a fixed $x_i\in\Omega_i^{\mathrm{m}}\cap[p_{4,i},\check{x}_i^{\mathrm{m}}]$, for each $\xi_i'\in\Omega_i^l$ (respectively, Ω_i^{m}), there exists $\xi_i\in\Omega_i^l$ (respectively, Ω_i^{m}) such that

$$x_i=\alpha\xi_i+\omega g_{\rho_i}(\xi_i)+\sum_{j=1,j\neq i}^{n}\omega_{ij}g_0(\xi_j')+a_i. \tag{4.6}$$

On the other hand, assume that (PC-1-a), (PC-1-b), and (PC-1-c(ii)) hold. Let $x_i\in\Omega_i^{\mathrm{r}}$ be fixed. For each $\xi_i'\in\Omega_i^{\mathrm{m}}$ (respectively, Ω_i^{r}), there exists $\xi_i\in\Omega_i^{\mathrm{m}}$ (respectively, Ω_i^{r}) such that

$$x_i=\alpha\xi_i+\omega g_{\rho_i}(\xi_i)+\sum_{j=1,j\neq i}^{n}\omega_{ij}g_0(\xi_j')+a_i. \tag{4.7}$$

Similarly, for a fixed $x_i\in\Omega_i^{\mathrm{m}}\cap[\hat{x}_i^{\mathrm{m}},p_{2,i}]$, for each $\xi_i'\in\Omega_i^{\mathrm{r}}$ (respectively, Ω_i^{m}), there exists $\xi_i\in\Omega_i^{\mathrm{r}}$ (respectively, Ω_i^{m}) such that

$$x_i=\alpha\xi_i+\omega g_{\rho_i}(\xi_i)+\sum_{j=1,j\neq i}^{n}\omega_{ij}g_0(\xi_j')+a_i. \tag{4.8}$$

(II) Consider the case (PC-1-a,-b,-c(i)). Let $\overline{\mathbf{x}}=(\overline{x_1},\ldots,\overline{x_n})$ be a fixed point in $\Omega_{j_1\cdots j_n}$, $j_i=$''l'' or ''m.'' Notice that if $j_i=$''m,'' then $\overline{x_i}\in\Omega_i^{\mathrm{m}}\cap[p_{4,i},\check{x}_i^{\mathrm{m}}]$. Let $(\xi_1',\ldots,\xi_n')\in\Omega_{j_1'\cdots j_n'}$, where $j_1',\ldots,j_n'$ are chosen as in (4.5), (4.6) so that there exists $(\xi_1,\ldots,\xi_n)\in\Omega_{j_1'\cdots j_n'}$, which satisfies

$$\overline{x_i}=\alpha\xi_i+\omega g_{\rho_i}(\xi_i)+\sum_{j=1,j\neq i}^{n}\omega_{ij}g_0(\xi_j')+a_i,$$

$$i=1,\ldots,n.$$

Define a map $G:\mathbb{R}^n\times\mathbb{R}^n\to\mathbb{R}^n$ by $G_i(\mathbf{x}',\mathbf{x})=\overline{x_i}-\alpha x_i-\omega g_{\rho_i}(x_i)-\Sigma_{j=1,j\neq i}^{n}\omega_{ij}g_0(x_j')-a_i$, $i=1,\ldots,n$. Then $(\partial G/\partial\mathbf{x})(\mathbf{x}',\mathbf{x})$ has the form (4.4) with $\chi_i=-\alpha-\omega g_{\rho_i}'(x_i)$, $i=1,\ldots,n$. Notice that $|\alpha+\omega g_{\rho_i}'(x_i)|\geq 1+(k_i/4\varepsilon)$ for $(x_1,\ldots,x_n)\in\Omega_{j_1'\cdots j_n'}$, according to (PC-1-a) and Lemma 3.1. It follows from similar arguments as the proof of theorem 4.1 that there exists a point $\tilde{\mathbf{x}}\in\Omega_{j_1'\cdots j_n'}$ such that $G(\tilde{\mathbf{x}},\tilde{\mathbf{x}})=0$. Denoting $\mathbf{x}^{-1}:=\tilde{\mathbf{x}}$, it follows that $F(\mathbf{x}^{-1})=\overline{\mathbf{x}}$. The case (PC-1-a, -b, -c(ii)) is similar.

(III) Let $\mathbf{x}^{-1}$ be as obtained in (II). Similar arguments as in (II) confirm that there exists $\mathbf{x}^{-2}\in\Omega_{j_1,\ldots,j_n}$ such that $F(\mathbf{x}^{-2})=\mathbf{x}^{-1}$. Continuously, we can find $\mathbf{x}^{-l}\in\Omega_{j_1,\ldots,j_n}$ with $l\geq 3$. Consider

$$DF(\mathbf{x})=\begin{pmatrix} \alpha+\omega g'_{\rho_1}(x_1) & \omega_{12}g'_0(x_2) & \cdots & \omega_{1n}g'_0(x_n) \\ \omega_{21}g'_0(x_1) & \alpha+\omega g'_{\rho_2}(x_2) & & \omega_{2n}g'_0(x_n) \\ \vdots & \vdots & \ddots & \vdots \\ \omega_{n1}g'_0(x_1) & \omega_{n2}g'_0(x_2) & \cdots & \alpha+\omega g'_{\rho_n}(x_n) \end{pmatrix}. \tag{4.9}$$

For each $i=1,\ldots,n$, let $r_i(\mathbf{x})=\Sigma_{j\neq i}^{n}|\omega_{ij}g'_0(x_j)|$. Then $r_i(\mathbf{x}) \leqslant \Sigma_{j\neq i}^{n}|\omega_{ij}(1/4\varepsilon)|<(k_i/4\varepsilon)$, since $0<g'_0(\xi)\leqslant(1/4\varepsilon)$ for all $\xi\in\mathbb{R}$. Thus, $||\alpha+\omega g'_{\rho_i}(x_i)|-r_i(\mathbf{x})|>1$ for each $i=1,\ldots,n$. By the compactness of $\Omega_{j_1\cdots j_n}$, there exists σ such that $\min_{i=1,\ldots,n}\{||\alpha+\omega g'_{\rho_i}(x_i)|-r_i(\mathbf{x})|\}>\sigma>1$, for all $\mathbf{x}\in\Omega_{j_1\cdots j_n}$. By the Gerschgorin's theorem, the absolute values of all eigenvalues of $DF(\mathbf{x})$ are larger than σ. It follows that the absolute values of all eigenvalues of $DF^{-1}(\mathbf{x})$ are less than $1/\sigma$. Hence, F is expanding on $\Omega_{j_1\cdots j_n}$ and F^{-1} is a contraction on $F(\Omega_{j_1\cdots j_n})$, under certain norm on $\mathbb{R}^n$. Therefore, the sequence $\{\mathbf{x}^{-l}\}$ lie on the unstable manifold of $\overline{\mathbf{x}}$ and $\mathbf{x}^{-l}\to\overline{\mathbf{x}}$. We thus conclude that the fixed point $\overline{\mathbf{x}}$ is a snap-back repeller. The orbit $\{\mathbf{x}^{-l}\}$ is exactly a transversal homoclinic orbit. In fact, $\overline{\mathbf{x}}$ is the only fixed point (a snap-back repeller) in $\Omega_{j_1\cdots j_n}$, as F is expanding on $\Omega_{j_1\cdots j_n}$. Consequently, for case (i), if (PC-1-c(i)) or (PC-2-c(i)) is satisfied, there exist at least 2^n snap-back repellers. Each of these repellers lies in one of the regions $\Omega_{j_1\cdots j_n}$, $j_i=$"l" or "m." If (PC-1-c(ii)) or (PC-2-c(ii)) is satisfied, there also exist at least 2^n snap-back repellers. Each of them lies in one of $\Omega_{j_1\cdots j_n}$, $j_i=$"m" or "r." Similarly, in case (ii), there exist 3^n snap-back repellers in $\mathbb{R}^n$. For case (iii), only the pre-images, hence the homoclinic orbits, for the middle fixed point in $\Omega_{\mathrm{m}\cdots\mathrm{m}}$ can be constructed. This completes the proof.

Our constructions in the proof of Theorem 4.2 show that there can be many different homoclinic orbits for a single snap-back repeller. The following descriptions sketch part of this scenario. Let us consider the two-dimensional TCNN. Assume that (PC-1-a, -b, -c(i), -c(ii)) hold and let $\overline{\mathbf{x}}_{\mathrm{mm}}$ be the fixed point in the middle region Ω_{mm}. By Theorem 4.2, we can find the pre-images of $\overline{\mathbf{x}}_{\mathrm{mm}}$ in the other eight regions in Fig. 13 [illustrating the case for (PC-1-a, -b, -c(i))]. For each of these pre-images, we can further find their pre-image in the region Ω_{mm}. Since F^{-1} is a contraction on $F(\Omega_{\mathrm{mm}})$, each point in Ω_{mm} will be iterated into the region $[\hat{x}_1^{\mathrm{m}},\check{x}_1^{\mathrm{m}}]\times[\hat{x}_2^{\mathrm{m}},\check{x}_2^{\mathrm{m}}]$ in some finite k steps under F^{-1}. As these pre-images of $\overline{\mathbf{x}}_{\mathrm{mm}}$ fall into the region $[\hat{x}_1^{\mathrm{m}},\check{x}_1^{\mathrm{m}}]\times[\hat{x}_2^{\mathrm{m}},\check{x}_2^{\mathrm{m}}]$, we can construct their further pre-images by two alternatives. One is to make them tend to the fixed point $\overline{\mathbf{x}}_{\mathrm{mm}}$ under F^{-1}. In doing so, we construct a transversal homoclinic orbit for $\overline{\mathbf{x}}_{\mathrm{mm}}$. The other one is to construct their further pre-images in any of the eight regions (excluding the region Ω_{mm} from the nine regions in Fig. 13). Same process can be continued. Thus, each of these homoclinic orbits for $\overline{\mathbf{x}}_{\mathrm{mm}}$ lies in the regions indexed by the following sequence:

$$\{*,\mathrm{mm},\mathrm{mm},\ldots,\mathrm{mm},*,\mathrm{mm},\mathrm{mm},\ldots,\mathrm{mm},\ldots,\ldots\}$$

where "mm" indexes the region Ω_{mm} and "*" represents one of the nine regions. Notice that F is an expansion in each of the nine regions. Therefore, for each point of a single transversal homoclinic orbit lying in the region Ω_{mm}, there exists exactly one pre-image in each of the other eight regions. We conclude that there exist infinitely many transversal homoclinic orbits for $\overline{\mathbf{x}}_{\mathrm{mm}}$.

Even if a snap-back repeller exists, the structure of this chaotic dynamics may not be included in an attractor. Thus, this chaotic phenomena may not be observable numerically. We shall attempt to derive trapping regions for (4.1) in the

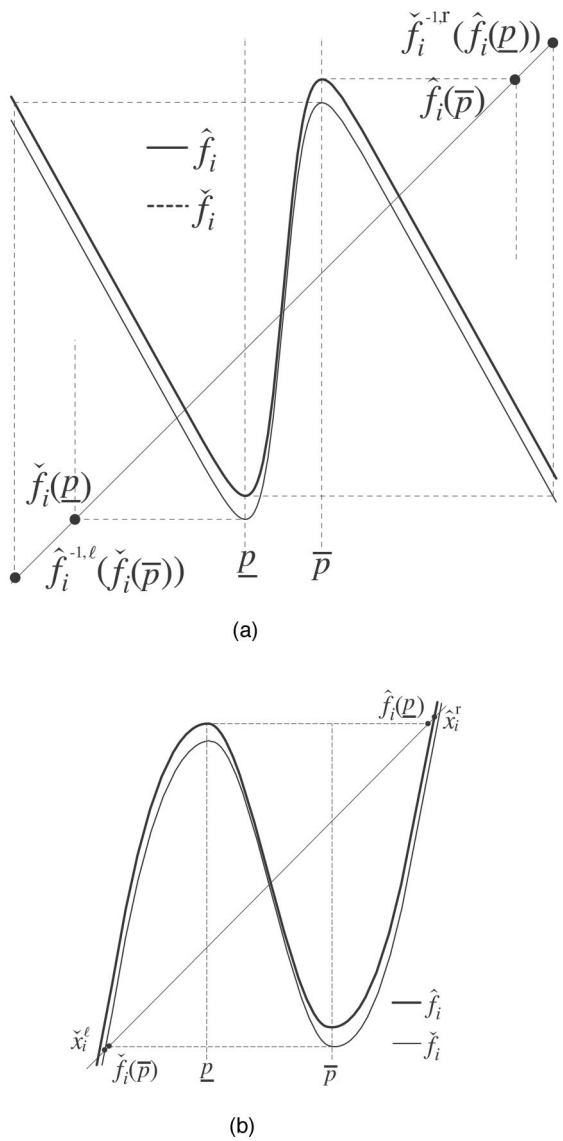

FIG. 14. Trapping regions for the i component of F. (a) Configuration under (PC-1-d). (b) Configuration under (PC-2-d).

following theorem. Let $\overline{p}$ and $\underline{p}$ be the two critical points of $\check{f}_i$ and of $\hat{f}_i$ with $\overline{p}>\underline{p}$, as shown in Figs. 14(a) and 14(b). Computation shows that $\overline{p}=\varepsilon L_+(\varepsilon\alpha)$, $\underline{p}=\varepsilon L_-(\varepsilon\alpha)$. Notably, $\overline{p}$ and $\underline{p}$ are independent of i,

$$\text{(PC-1-d)}\quad \check{f}_i(\hat{f}_i(\overline{p}))>\hat{f}_i(\underline{p}),\hat{f}_i(\check{f}_i(\underline{p}))<\check{f}_i(\overline{p}),\quad i=1,\ldots,n.$$

$$\text{(PC-2-d)}\quad g_{\rho_i}(\hat{f}_i(\underline{p}))>\frac{1-\alpha}{\omega}\hat{f}_i(\underline{p})-\frac{k_i}{\omega},\quad g_{\rho_i}(\check{f}_i(\overline{p}))<\frac{1-\alpha}{\omega}\check{f}_i(\overline{p})+\frac{k_i}{\omega},\quad i=1,\ldots,n.$$

Theorem 4.3. Assume that for $i=1,\ldots,n$, the parameters $(\varepsilon,\alpha,\omega,\rho_i,k_i)$ satisfy (PC-1-a, -b, -d) [respectively, (PC-2-a, -b, -d)]. Then $T:=[\check{f}_1(\underline{p}),\hat{f}_1(\overline{p})]\times\cdots\times[\check{f}_n(\underline{p}),\hat{f}_n(\overline{p})]$ [respectively, $[\check{f}_1(\overline{p}),\hat{f}_1(\underline{p})]\times\cdots\times[\check{f}_n(\overline{p}),\hat{f}_n(\underline{p})]$] is a trapping region for (4.1) in $\mathbb{R}^n$.

Proof. Each component $F_i(\mathbf{x})$ of $F(\mathbf{x})$ satisfies (4.2). Let $\mathbf{x}=(x_1,\ldots,x_n)\in T$. Notably, (PC-1-d) implies $[\check{f}_i(\underline{p}),\hat{f}_i(\overline{p})]\subset[\hat{f}_i^{-1,l}(\check{f}_i(\overline{p})),\check{f}_i^{-1,\mathrm{r}}(\hat{f}_i(\underline{p}))]$. It follows that for each i, if $x_i\in[\check{f}_i(\underline{p}),\hat{f}_i(\overline{p})]$, then $F_i(\mathbf{x})\in[\check{f}_i(\underline{p}),\hat{f}_i(\overline{p})]$. We thus conclude that $F(T)\subset T$, see Fig. 14(a).

With a graph similar to Fig. 5, it can be observed that the first condition of (PC-2-d) guarantees $\hat{f}_i(\underline{p})<\hat{x}_i^{\mathrm{r}}$, where $\hat{x}_i^{\mathrm{r}}$ is the right fixed point of $\hat{f}_i$, and the second condition of (PC-2-d) yields $\check{f}_i(\overline{p})>\check{x}^l$, where $\check{x}^l$ is the left fixed point of $\check{f}_i$. For each i, $[\check{f}_i(\overline{p}),\hat{f}_i(\underline{p})]=[\check{f}_i(\overline{p}),\underline{p}]\cup[\underline{p},\overline{p}]\cup[\overline{p},\hat{f}_i(\underline{p})]$. For each i, if $x_i\in[\underline{p},\overline{p}]$, then $F_i(\mathbf{x})\in[\check{f}_i(\overline{p}),\hat{f}_i(\underline{p})]$. For each i, if $x_i\in[\overline{p},\hat{f}_i(\underline{p})]$, then $F_i(\mathbf{x})\in[\check{f}_i(\overline{p}),\hat{f}_i(\underline{p})]$, by the above observation, see Fig. 14(b). Similarly, if $x_i\in[\check{f}_i(\overline{p}),\underline{p}]$, then $F_i(\mathbf{x})\in[\check{f}_i(\overline{p}),\hat{f}_i(\underline{p})]$. This completes the proof.

As the snap-back repellers and the trapping regions for (4.1) are considered together, the situation becomes different for (PC-1) and (PC-2). One can find parameters $(\varepsilon,\alpha,\omega,\rho_i,k_i)$ that satisfy (PC-1-a, -b, -c(i), -c(ii)) as well as (PC-1-d). However, there do not exist parameters which satisfy (PC-2-d) and (PC-2-c(i)) or (PC-2-c(ii)). As depicted in Fig. 7, when (PC-2-c(i)) holds, the left-lower block is higher than the value of the function $\check{f}_i$ at $\overline{p}$, and when (PC-2-c(ii)) holds, the right-upper block is lower than the value of the function $\hat{f}_i$ at $\underline{p}$. Accordingly, there are points in $[\check{f}_i(\overline{p}),\hat{f}_i(\underline{p})]$ escaping from this interval after some iterations. On the other hand, if (PC-2-d) holds, then we have a situation like Fig. 8. Under the circumstances, we can only construct the pre-images for the middle fixed point. Therefore, (PC-2-d) is compatible with (PC-2-c(iii)) or (PC-2-c(iv)), but not (PC-2-c(i), (ii)).

All of the above results can be generalized to the map $F=(F_1,\ldots,F_n)$ with $F_i(\mathbf{x})=\alpha_i x_i+\omega_{ii}g_{\rho_i}(x_i)+\Sigma_{j=1,j\neq i}^n\omega_{ij}g_0(x_j)+a_i$. Restated, α and ω can be different for each component of F. The upper and lower maps $\hat{f}_i,\check{f}_i$ are then adjusted to

$$\hat{f}_i(x)=\alpha_i x+\omega_{ii}g_{\rho_i}(x)+k_i,$$

$$\check{f}_i(x)=\alpha_i x+\omega_{ii}g_{\rho_i}(x)-k_i.$$

V. ASYMPTOTIC CONVERGENCE FOR TCNN

Certain sufficient conditions on the existence of a Lyapunov function, hence asymptotic convergence to fixed points, for (1.4) with symmetric $[\omega_{ij}]$, have been derived in Ref. 8. The purpose of this section is to give precise statement of the convergence theorem and to demonstrate the extension of the theorem to TCNN with cycle-symmetric connections.[17] In addition, it is interesting to compare the convergent regime and the chaotic regime for (1.2), (1.4).

An $n\times n$ matrix $A=[a_{ij}]$ is said to be cycle-symmetric if it is sign-symmetric ($a_{ij}a_{ji}>0$, if $a_{ij}\neq 0$, $a_{ji}=0$ if $a_{ij}=0$), and $\Pi_C a_{ij}=\Pi_C a_{ji}$, along every cycle C (Π means product). Such class of matrices is a generalization of symmetric matrices. Indeed, if A is cycle-symmetric, then there exists an invertible diagonal matrix P such that PBP^{-1} is symmetric, cf. Ref. 17 and the references therein.

Let $W=[\omega_{ij}]$ be the $n\times n$ matrix with its (i,j)-entry the connection weight from neuron i to neuron j. Assume that W is cycle-symmetric, and $P=\mathrm{diag}[p_1,\ldots,p_n]$ is a diagonal matrix which symmetrizes W, that is, $PWP^{-1}=\tilde{W}=[\tilde{\omega}_{ij}]$ is symmetric. Then a change of variables $\tilde{\mathbf{x}}=P\mathbf{x}$ transforms (1.4) to

$$\tilde{x}_i(t+1)=\alpha\tilde{x}_i(t)+\omega_{ii}[\tilde{y}_i(t)-\tilde{a}_{0i}]+\sum_{j=1,j\neq i}^n\tilde{\omega}_{ij}\tilde{y}_j(t)+\tilde{a}_i,\tag{5.1}$$

where $\tilde{y}_j=h_j(\tilde{x}_j):=p_j g_0(p_j^{-1}\tilde{x}_j)$, $\tilde{a}_i=p_i a_i$, $\tilde{a}_{0i}=p_i a_{0i}$. Notably, each p_j can be chosen positive and thus h_j is strictly increasing and has similar property as g_0.

For notational convenience, we drop the "tilde" in (5.1). Consider the following function:

$$V(\mathbf{x})=-\frac{1}{2}\sum_{i,j=1}^n\omega_{ij}h_i(x_i)h_j(x_j)-\sum_{i=1}^n(a_i-a_{0i}\omega_{ii})h_i(x_i)-(\alpha-1)\sum_{i=1}^n\int_0^{h_i(x_i)}h_i^{-1}(\xi)d\xi.\tag{5.2}$$

Let us elaborate on the following computations:

$$\begin{aligned}V(\mathbf{x}(t+1))-V(\mathbf{x}(t))&=-\frac{1}{2}\sum_{i,j=1}^n\omega_{ij}\Delta y_i\Delta y_j-\frac{1}{2}\sum_{i,j=1}^n\omega_{ij}[y_i(t)\Delta y_j+y_j(t)\Delta y_i]-\sum_{i=1}^n\Delta y_i\\&\times\left[x_i(t+1)-\alpha x_i(t)-\sum_{j=1}^n\omega_{ij}y_j(t)\right]+(1-\alpha)\sum_1^n\int_{y_i(t)}^{y_i(t+1)}h_i^{-1}(\xi)d\xi\end{aligned}\tag{5.3}$$

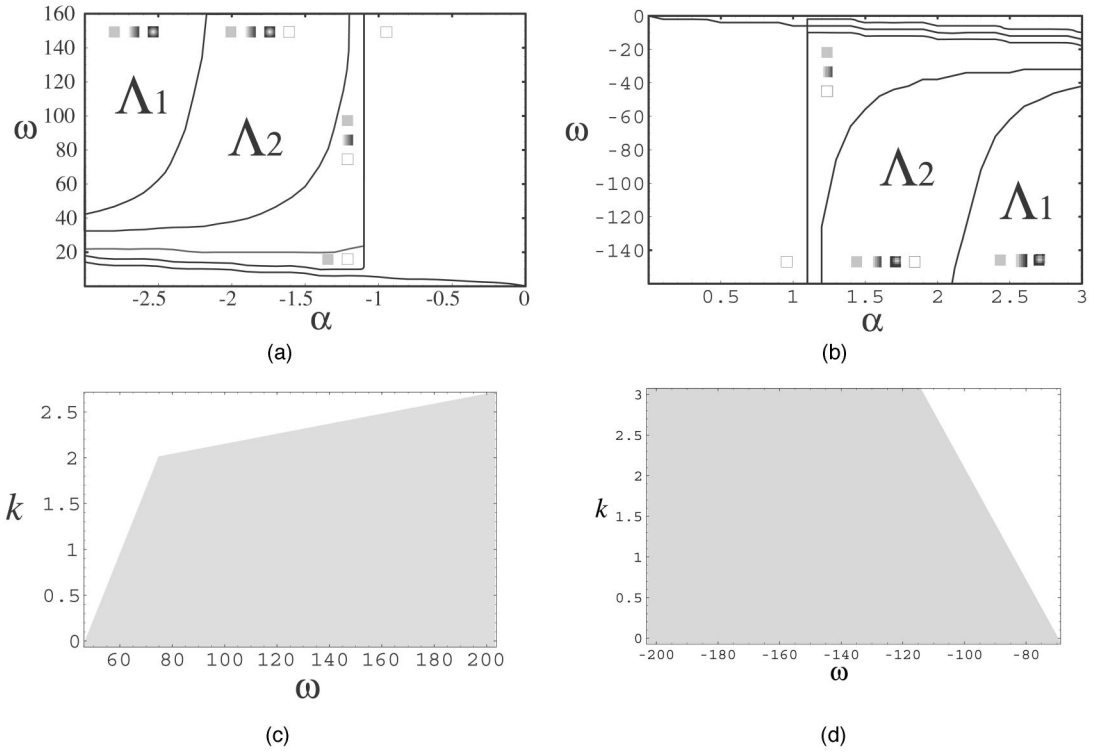

FIG. 15. (a) and (b) describe the parameter ranges for (α,ω) with fixed $\varepsilon=1$, $\rho=0.55$, $k=0$. There exist three snap-back repellers in regions Λ_1 and Λ_2. Marotto's chaos is observable numerically in region Λ_2. (a) (PC-1) case: Locate the parameters (α,ω) which satisfy conditions (PC-1-a,-b,-c(i)(ii),-d). (b) (PC-2) case: Locate the parameters (α,ω) which satisfy conditions (PC-2-a,-b,-c(iii)(iv),-d). (c) and (d) describe the parameter ranges for (ω,k) with fixed $\alpha=-1.8$, $\varepsilon=1$, $\rho=0.55$, and fixed $\alpha=1.8$, $\varepsilon=1$, $\rho=0.55$, respectively. (c) Locate the parameters (ω,k) which satisfy conditions (PC-1-a,-b,-c(i)(ii),-d). (d) Locate the parameters (ω,k) which satisfy conditions (PC-2-a,-b,-c(iii)(iv),-d).

$$= -\frac{1}{2}\sum_{i,j=1}^{n}\omega_{ij}\Delta y_i\Delta y_j-\sum_{i=1}^{n}\Delta y_i[x_i(t+1) - \alpha x_i(t)]+(1-\alpha)\sum_{1}^{n}\int_{y_i(t)}^{y_i(t+1)}h_i^{-1}(\xi)d\xi \tag{5.4}$$

$$\leqslant -\frac{1}{2}\sum_{i,j=1}^{n}\omega_{ij}\Delta y_i\Delta y_j-(1-\alpha) \times\sum_{i=1}^{n}\left[\Delta y_i x_i(t+1)-\int_{y_i(t)}^{y_i(t+1)}h_i^{-1}(\xi)d\xi\right] \tag{5.5}$$

$$\leqslant -\frac{1}{2}\sum_{i,j=1}^{n}\omega_{ij}\Delta y_i\Delta y_j-2\varepsilon(1-\alpha)\sum_{i=1}^{n}(\Delta y_i)^2, \tag{5.6}$$

where $\Delta y_i=y_i(t+1)-y_i(t)$. We have used symmetry of $[\omega_{ij}]$ in obtaining (5.4). Since h_i is increasing, (5.5) is derived from $\alpha\Delta y_i[x_i(t+1)-x_i(t)]=\alpha[h_i(x_i(t+1))-h_i(x_i(t))][x_i(t+1)-x_i(t)]\geqslant 0$ for $\alpha\geqslant 0$. Using Taylor's expansion and estimating the maximum of h_i' yield (5.6). These computations resemble the ones in Ref. 8. We merely generalize them to cycle-symmetric W, as well as indicate that these calculations also work for output functions h_i, instead of just g_0. We thus derive the following Proposition, cf. Theorem 4.1 and Remark 4.1 in Ref. 8.

Proposition 5.1. Assume that W is cycle-symmetric, $\varepsilon>0$, and (i) $0\leqslant\alpha\leqslant 1$, $\omega_{ii}+4(1-\alpha)\varepsilon>\Sigma_{j=1,j\neq i}^{n}|\omega_{ij}|$, $i=1,\ldots,n$, or (ii) $\alpha>1$, $\omega_{ii}+8\varepsilon>\Sigma_{j=1,j\neq i}^{n}|\omega_{ij}|$, $i=1,\ldots,n$. Then V defined by (5.2) is nonincreasing along every orbit of (1.4). Moreover, $\mathcal{S}:=\{\mathbf{x}|V(F(\mathbf{x}))=V(\mathbf{x})\}$ consists of fixed points for (1.4).

Proof. That V is nonincreasing along every orbit of (5.1) has been shown in (5.3)–(5.6) for case (i). Case (ii) is similar. Under conditions in (i), we have (5.6)$=0$ if and only if $\Delta y_i=y_i(t+1)-y_i(t)=0$ for every i. In addition, the equalities in (5.6) and (5.5) hold if and only if $\Delta y_i=0$ for every i. Thus $\mathcal{S}=\{$all fixed points (1.4)$\}$. The proof is completed.

The following theorem can be concluded by the La-Salle's invariance principle. This result was not clearly stated in Ref. 8.

Theorem 5.2. Under the conditions of Proposition 5.1, every bounded orbit of (1.4) converges to the set of fixed points of (1.4).

Let us compare the parameter conditions in Secs. III and IV, with the two conditions in Proposition 5.1. Since $\alpha\geqslant 0$ in Proposition 5.1, we only make this comparison in the context of (PC-2-a). Recall that $k_i=\Sigma_{j=1,j\neq i}^{n}(|\omega_{ij}|+|a_i|)$. Assume that W is symmetric, and each $(\varepsilon,\alpha,\omega_{ii},\rho_i,k_i)$ satisfies (PC-2-a), the second part of (PC-2-a) yields $\omega_{ii}+8\varepsilon<-4\varepsilon\alpha-k_i<-k_i\leqslant-\Sigma_{j=1,j\neq i}^{n}|\omega_{ij}|$. A comparison to (ii) of Proposition 5.1 distinguishes between the chaotic regime and the convergent regime for (1.4).

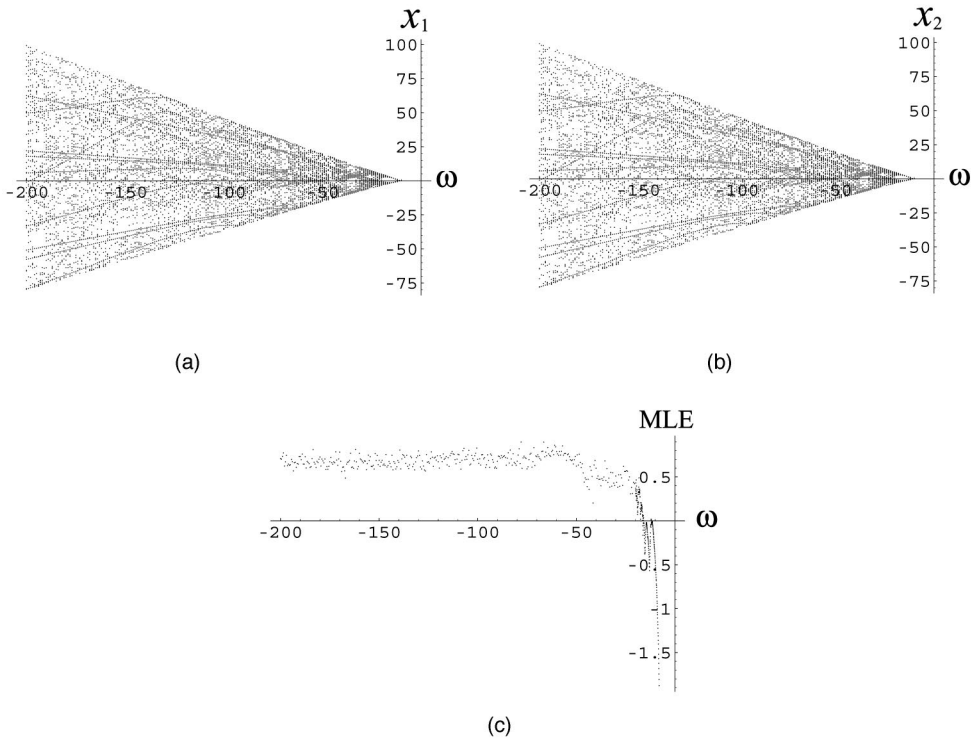

FIG. 16. (a) and (b) are the bifurcation diagrams for the iterations of x_1 and x_2. (c) The maximum Lyapunov exponent for a range of ω.

VI. NUMERICAL ILLUSTRATIONS

In this section, we shall illustrate the numerical ranges for the parameters satisfying Theorems 4.2 and 4.3. The Lyapunov exponents for TCNN with the parameters in these ranges will also be computed.

It is not difficult to write a computer program (for example, using Mathematica software) to locate the parameters satisfying the parameter conditions (PC-j-a, -b, -c, -d), j $=1, 2$. Figure 15 gives such an illustration. In order to make the computations comprehensible, we present the numerical ranges of these parameters on two-dimensional parameter spaces. Restated, we first fix three of the five parameters $(\varepsilon,\alpha,\omega,\rho,k)$ and locate the ranges of the other two parameters satisfying (PC-j-a,-b,-c,-d), $j=1,2$. In Fig. 15(c) [respectively, Fig. 15(a)], the parameters (ω,k) [respectively, (α,ω)] in the shaded region satisfy (PC-1-a,-b,-c(i),(ii),-d) with fixed $\alpha=-1.8$, $\varepsilon=1$, $\rho=0.55$ (respectively, with fixed $k=0$, $\varepsilon=1$, $\rho=0.55$). In Fig. 15(d) [respectively, 15(b)], the parameters (ω,k) [respectively, (α,ω)] in the shaded region satisfy (PC-2-a,-b,-c(iii), (iv),-d) with fixed $\alpha=1.8$, $\varepsilon=1$, $\rho=0.55$ (respectively, with $k=0$, $\varepsilon=1$, $\rho=0.55$).

Example 6.1. Consider a two-dimensional case of (1.4), that is, the two-dimensional TCNN. Let $\alpha=1.8$, $\omega_{11}=\omega_{22}=\omega(<0)$, $\omega_{12}=-0.5$, $\omega_{21}=0.5$, $\varepsilon=1$, $a_{01}=0.55$, $a_{02}=0.55$, $a_1=a_2=0$. These parameters correspond to the ranges in Fig. 15(d). Figures 16(a) and 16(b) are the bifurcation diagrams for the iterations of x_1 and x_2, with respect to ω. Figure 16(c) shows the maximum Lyapunov exponent (MLE) for ω ranging from -200 to -8. The parameters in this example satisfy (PC-2-d). Therefore, there exists a trapping region due to Theorem 4.3. In addition, these parameters with $\omega\in(-200,-70)$ also satisfy (PC-2-a), (PC-2-b), (PC-2-c(iii)), and (PC-2-c(iv)). Hence, there exists a snap-back repeller in $\Omega_{\rm mm}$, according to Theorem 4.2.

Example 6.2. Consider the two-dimensional TCNN with $\alpha=1.3$, $\omega_{11}=\omega_{22}=\omega(<0)$, $\omega_{12}=-0.5$, $\omega_{21}=0.5$, $\varepsilon=1/250$, $a_{01}=0.48$, $a_{02}=0.55$, $a_1=a_2=0$. These parameter values have been used in Ref. 7. The bifurcation diagrams which are similar to Fig. 16 and computations of the maximum Lyapunov exponents can be found in Ref. 7.

VII. CONCLUSIONS

This paper has theoretically proved that TCNN has chaotic structure by applying Marotto' theorem and has given sufficient conditions for the existence of both fixed points and their homoclinic orbits. The analysis has indicated that, as multiple fixed points coexist, their homoclinic orbits position themselves in a tangle. In addition, the number of fixed points can grow exponentially in the number of neurons (the size of the system). This scenario has revealed the complication of the dynamics for the system. It is believed that more dynamical features other than snap-back repellers can be explored along this line of investigation. This study has also provided basic numerical ranges for the parameters which correspond to chaotic dynamics of TCNN. Computations of these numerical ranges were also illustrated. It is expected that the methodology used in this multi-dimensional map can be applied to other dynamical systems.

ACKNOWLEDGMENTS

This work is partially supported by The National Science Council and The National Center of Theoretical Sciences of R.O.C. on Taiwan.

APPENDIX A

Recall the definitions of L_- and L_+ in (3.3), (3.4),

$$L_+(\eta) := \mathrm{Log}\frac{2\eta}{-2\eta-\omega+\sqrt{\omega}\sqrt{4\eta+\omega}}, \tag{A1}$$

$$L_-(\eta) := \mathrm{Log}\frac{2\eta}{-2\eta-\omega-\sqrt{\omega}\sqrt{4\eta+\omega}}. \tag{A2}$$

Lemma A.1. (i) If $\omega>0$, then for $-\omega/4<\eta<0$, (a) $\mathrm{Exp}(L_+(\eta))>1$, $0<\mathrm{Exp}(L_-(\eta))<1$; (b) $L_+(\eta)$ is a positive increasing function; (c) $L_-(\eta)$ is a negative decreasing function. (ii) If $\omega<0$, then for $0<\eta<-\omega/4$, (a) $\mathrm{Exp}(L_+(\eta))>1$, $0<\mathrm{Exp}(L_-(\eta))<1$; (b) $L_+(\eta)$ is a positive decreasing function; (c) $L_-(\eta)$ is a negative increasing function.

Proof: For (i-a),

$$\begin{aligned}
&4\eta+\omega>0 \Rightarrow -4\eta-\omega<\sqrt{\omega}\sqrt{4\eta+\omega}\\
&\quad\Leftrightarrow -2\eta-\omega-\sqrt{\omega}\sqrt{4\eta+\omega}<2\eta\\
&\quad\Leftrightarrow \frac{-2\eta-\omega-\sqrt{\omega}\sqrt{4\eta+\omega}}{2\eta}>1.
\end{aligned}$$

Moreover,

$$\begin{aligned}
&4\eta^2>0 \Leftrightarrow 4\eta^2+4\eta\omega+\omega^2>4\eta\omega+\omega^2=\omega(4\eta+\omega)\\
&\quad\Leftrightarrow (2\eta+\omega)^2>(\sqrt{\omega})^2(\sqrt{4\eta+\omega})^2\\
&\quad\Leftrightarrow 2\eta+\omega>\sqrt{\omega}\sqrt{4\eta+\omega}\\
&\quad\Leftrightarrow 2\eta+\omega-\sqrt{\omega}\sqrt{4\eta+\omega}>0\\
&\quad\Leftrightarrow \frac{-2\eta-\omega+\sqrt{\omega}\sqrt{4\eta+\omega}}{2\eta}>0,
\end{aligned}$$

$$\begin{aligned}
&\sqrt{\omega}>\sqrt{4\eta+\omega} \Leftrightarrow \sqrt{\omega}\sqrt{4\eta+\omega}>(\sqrt{4\eta+\omega})^2=4\eta+\omega\\
&\quad\Leftrightarrow -2\eta-\omega+\sqrt{\omega}\sqrt{4\eta+\omega}>2\eta\\
&\quad\Leftrightarrow \frac{-2\eta-\omega+\sqrt{\omega}\sqrt{4\eta+\omega}}{2\eta}<1.
\end{aligned}$$

For a negative number b, $\sqrt{b}$ means $i\sqrt{-b}$. (ii-a) follows from the following computations:

$$\begin{aligned}
&4\eta+\omega<0 \Rightarrow 4\eta+\omega<\sqrt{-\omega}\sqrt{-4\eta-\omega}\\
&\quad\Leftrightarrow -2\eta-\omega-\sqrt{\omega}\sqrt{4\eta+\omega}>2\eta\\
&\quad\Leftrightarrow \frac{-2\eta-\omega-\sqrt{\omega}\sqrt{4\eta+\omega}}{2\eta}>1,
\end{aligned}$$

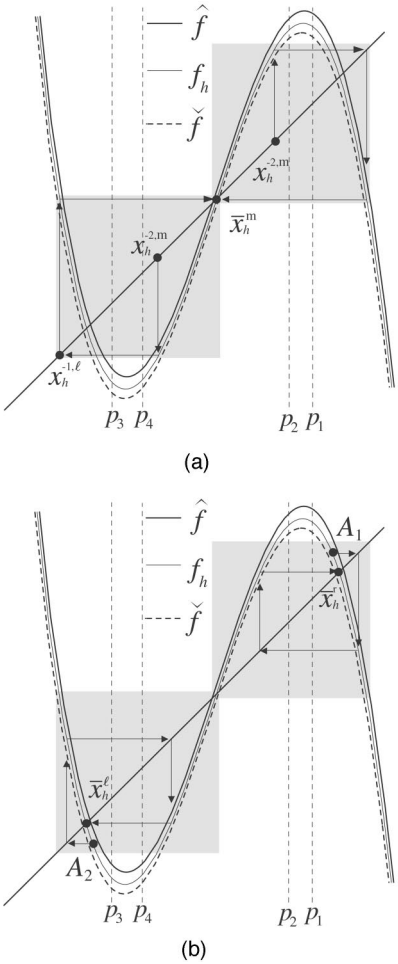

FIG. 17. In the two figures (a) and (b), the left-lower shaded region satisfies (PC-1-a,-b,-c(i)), and the right-upper shaded region satisfies (PC-1-a,-b, -c(ii)). (a) Two snap-back points $x_h^{-2,m}$ for repeller $\bar{x}_h^{m}$. (b) The first coordinate of point A_1 (respectively, A_2) is a snapback point for the snapback repeller $\bar{x}_h^{r}$ (respectively, $\bar{x}_h^{t}$).

$$\begin{aligned}
&4\eta^2>0 \Leftrightarrow 4\eta^2+4\eta\omega+\omega^2>4\eta\omega+\omega^2\\
&\quad\Leftrightarrow (2\eta+\omega)^2>(\sqrt{-\omega})^2(\sqrt{-4\eta-\omega})^2\\
&\quad\Leftrightarrow -(2\eta+\omega)>\sqrt{-\omega}\sqrt{-4\eta-\omega}\\
&\quad\Leftrightarrow -2\eta-\omega+\sqrt{\omega}\sqrt{4\eta+\omega}>0\\
&\quad\Leftrightarrow \frac{-2\eta-\omega+\sqrt{\omega}\sqrt{4\eta+\omega}}{2\eta}>0,
\end{aligned}$$

$$\begin{aligned}
&\sqrt{-\omega}>\sqrt{-4\eta-\omega} \Leftrightarrow \sqrt{-\omega}\sqrt{-4\eta-\omega}>(\sqrt{-4\eta-\omega})^2\\
&\quad=-4\eta-\omega\\
&\quad\Leftrightarrow -2\eta-\omega+\sqrt{\omega}\sqrt{4\eta+\omega}<2\eta\\
&\quad\Leftrightarrow \frac{-2\eta-\omega+\sqrt{\omega}\sqrt{4\eta+\omega}}{2\eta}<1.
\end{aligned}$$

(i-b), (i-c), (ii-b), and (ii-c) follow from $L'_-(\eta)=[\sqrt{\omega}/(\eta\sqrt{\omega+4\eta})]$ and $L'_+(\eta)=-[\sqrt{\omega}/(\eta\sqrt{\omega+4\eta})]$.

Proof of Lemma 3.1: For case (i), since $\varepsilon>0$, $\varepsilon(1+\alpha+(k/4\varepsilon))<0$, $\omega>0$, $4\varepsilon(-1+\alpha-(k/4\varepsilon))+\omega>0$, p_1, p_2, p_3, and p_4 are well defined, where $f'(p_2)=f'(p_4)=1$

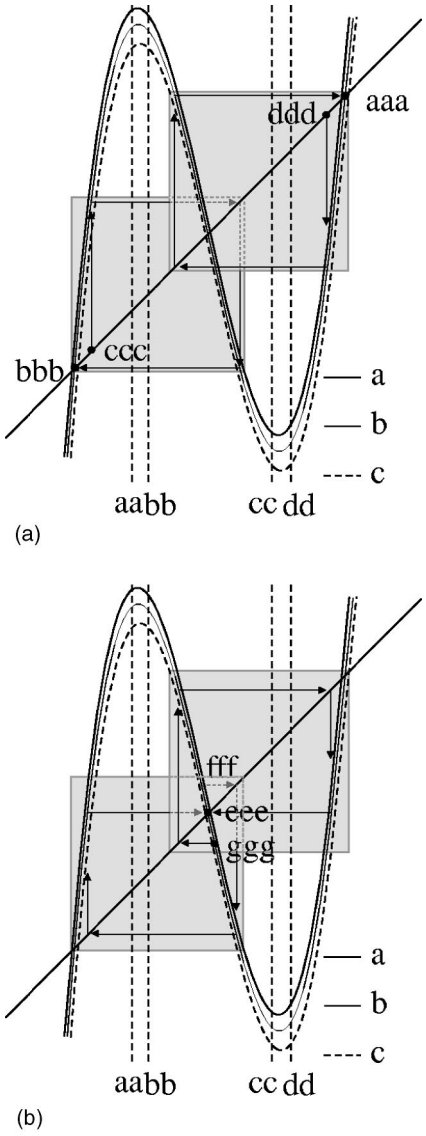

FIG. 18. In the two figures (a) and (b), the left-lower shaded region satisfies (PC-2-a,-b,-c(i)) and the right-upper shaded region satisfies (PC-2-a,-b,-c(ii)). (a) $x_h^{-2,l}$ (respectively, $x_h^{-2,\mathrm{r}}$) is a snap-back point for the snapback repeller $\overline{x}_h^{+}$ (respectively, $\overline{x}_h^{\mathrm{r}}$). (b) The first coordinates of points A_1 and A_2 are snap-back points for $\overline{x}_h^{\mathrm{m}}$.

$+(k/4\varepsilon)$ and $f'(p_1)=f'(p_3)=-1-(k/4\varepsilon)$. By Lemma A.1.(i), we obtain $p_1>p_2>p_4>p_3$. Furthermore, computation shows that $f''(x)<0$ for $x>0$, $f''(x)>0$ for $x<0$ and $f''(0)=0$. Therefore, if $p_4<x<p_2$, then $f'(x)>1+(k/4\varepsilon)$. If $x>p_1$ or $x<p_3$, then $f'(x)<-1-(k/4\varepsilon)$. The verification for case (ii) is similar.

Proof of Proposition 3.4: (i) It follows from Lemma 3.1(i) that p_1, p_2, p_3, and p_4 exist and $p_1>p_2>p_4>p_3$. By (PC-1-b), each of $\hat{f}$ and $\check{f}$ has three fixed points, see Fig. 5. Since $\check{f}\leqslant f_h\leqslant\hat{f}$, f_h also has three fixed points $\overline{x}_h^{+}\in\tilde{\Omega}^{l}$, $\overline{x}_h^{\mathrm{m}}\in\tilde{\Omega}^{\mathrm{m}}$, and $\overline{x}_h^{\mathrm{r}}\in\tilde{\Omega}^{\mathrm{r}}$.

(ii) Let $x_h^{-n,\mathrm{m}}$ represent the pre-image of $x_h^{-n+1,\mathrm{m}}$ under f_h and lying in $\tilde{\Omega}^{\mathrm{m}}$ $(n>1)$. Assume that (PC-1-a), (PC-1-b), and (PC-1-c(i)) hold. First, let us consider the left-lower block in Figs. 7(a) and 17(a). In this block $[\check{f}^{-1,l}(\check{x}^{\mathrm{m}}),\check{x}^{\mathrm{m}}]\times[\check{f}^{-1,l}(\check{x}^{\mathrm{m}}),\check{x}^{\mathrm{m}}]$, we can find $x_h^{-1,l}\in\tilde{\Omega}^{l}$ such that $f_h(x_h^{-1,l})=\overline{x}_h^{\mathrm{m}}$ and $x_h^{-2,\mathrm{m}}\in\tilde{\Omega}^{\mathrm{m}}$ such that $f_h^2(x_h^{-2,\mathrm{m}})=f_h(x_h^{-1,l})=\overline{x}_h^{\mathrm{m}}$ [see Fig. 17(a)]. Since $f_h'(x)$ is larger than $1+(k/4\varepsilon)$ for $x\in\tilde{\Omega}^{\mathrm{m}}$, f_h^{-1} is a contraction on $f_h(\tilde{\Omega}^{\mathrm{m}})$. Thus, there exists a sequence $\{x_h^{-1,l},x_h^{-2,\mathrm{m}},\ldots,x_h^{-n,\mathrm{m}},\ldots\}$ such that $x_h^{-n,\mathrm{m}}\to\overline{x}_h^{\mathrm{m}}$ as $n\to\infty$. This sequence is a transversal homoclinic orbit for $\overline{x}_h^{\mathrm{m}}$. Hence, (PC-1-a, -b, -c(i)) imply that $\overline{x}_h^{\mathrm{m}}$ is a snap-back repeller. Analogous arguments justify that $\overline{x}_h^{+}$ is a snap-back repeller. Its homoclinic orbit is as illustrated in Fig. 17(a). For the conditions (PC-2-a), (PC-2-b), and (PC-2-c(i)), the left-lower blocks of Figs. 18(a) and 18(b) demonstrate the constructions of pre-images for the fixed points $\overline{x}_h^{+}$ and $\overline{x}_h^{\mathrm{m}}$.

(iii) For conditions (PC-1-a), (PC-1-b), and (PC-1-c(ii)), the right-upper square in Figs. 17(a) and 17(b) explain why $\overline{x}_h^{\mathrm{m}}$ and $\overline{x}_h^{\mathrm{r}}$ are snap-back repellers. For (PC-2-a), (PC-2-b), and (PC-2-c(ii)), the scenario for $\overline{x}_h^{\mathrm{m}}$ and $\overline{x}_h^{\mathrm{r}}$ being snap-back repellers can be explained by the orbits in the right-upper square in Figs. 18(a) and 18(b).

(iv) The pre-images for the fixed point $\overline{x}_h^{\mathrm{m}}$ of f_h can be constructed similarly, see the configuration in Fig. 8(b).

APPENDIX B: GERSCHGORIN'S THEOREM

Consider a matrix

$$A=\begin{pmatrix} a_{11} & \cdots & a_{1n} \\ \vdots & \ddots & \vdots \\ a_{n1} & \cdots & a_{nn} \end{pmatrix}.$$

Let $\lambda_p\in\mathbb{C}$, $p=1,\ldots,n$, be eigenvalues of A, and let $\theta_i=a_{ii}$, $r_i=\Sigma_{j\neq i}^{n}|a_{ij}|$, $i=1,\ldots,n$. Then $\lambda_p\in\cup_{i=1}^{n}B(\theta_i;r_i)$, $p=1,\ldots,n$.

APPENDIX C: MAROTTO'S THEOREM

Let us define a system as $X_{k+1}=F(X_k)$ where $X_k\in\mathbb{R}^n$, and $F\in C^1(\mathbb{R}^n,\mathbb{R}^n)$. A fixed point $\overline{X}$ is said to be a *snap-back repeller* of F if there exists a real number $r(>0)$ and $X_0\in B(\overline{X};r)$ with $X_0\neq\overline{X}$ such that all eigenvalues of $DF(X)$ exceed unity in norm for all $X\in B(\overline{X};r)$ and $F^m(X_0)=\overline{X}$ with $\det(DF^m(X_0))\neq 0$ for some positive integer m. If F has a snap-back repeller, then the system of F is chaotic in the following sense: (1) There exists a positive integer m_0 such that for each integer $p\geqslant m_0$, F has p-periodic points. (2) There exists a scrambled set, that is, an uncountable set L containing no periodic points such that the following pertains: (a) $F(L)\subset L$; (b) for every $Y\in L$ and any periodic point X of F,

$$\limsup_{m\to\infty}\|F^m(Y)-F^m(X)\|>0;$$

(c) for every $X,Y\in L$ with $X\neq Y$,

$$\limsup_{m\to\infty}\|F^m(Y)-F^m(X)\|>0.$$

(3) There exists an uncountable subset L_0 of L such that for every $X,Y\in L_0$,

$$\liminf_{m\to\infty}\|F^m(Y)-F^m(X)\|=0.$$

[1] M. A. Cohen and S. Grossberg, IEEE Trans. Syst. Man Cybern. **SMC-13**, 815 (1983).
[2] J. Hopfield, Proc. Natl. Acad. Sci. U.S.A. **81**, 3088 (1984).
[3] J. Hopfield and D. Tank, Biol. Cybern. **52**, 141 (1985).
[4] C. Peterson and J. R. Anderson, Complex Syst. **1**, 995 (1989).
[5] C. Peterson and B. Söderberg, ''Artificial neural networks,'' in *Modern Heuristic Techniques for Combinatorial Optimization*, edited by C. Reeves (Blackwell Scientific, Oxford, England, 1993), pp. 197–242.
[6] L. Chen and K. Aihara, Neural Networks **8**, 915 (1995).
[7] L. Chen and K. Aihara, IEEE Trans. Circuits Syst., I: Fundam. Theory Appl. **46**, 974 (1999).
[8] L. Chen and K. Aihara, Physica D **104**, 286 (1997).
[9] F. R. Marotto, J. Math. Anal. Appl. **63**, 199 (1978).
[10] G. Chen, S. B. Hsu, and J. Zhou, J. Math. Phys. **39**, 6459 (1998).
[11] T. Y. Li and J. A. Yorke, Am. Math. Monthly **82**, 985 (1975).
[12] F. R. Marotto, J. Math. Anal. Appl. **72**, 716 (1979).
[13] F. R. Marotto, Commun. Math. Phys. **68**, 187 (1979).
[14] S. S. Chen and C. W. Shih (unpublished).
[15] J. P. LaSalle, *The Stability of Dynamical Systems*, Regional Conference Series in Applied Mathematics, Vol. 25 (SIAM, Philadelphia, 1976).
[16] K. Meyer and X. Zhang, J. Diff. Eqns. **132**, 66 (1996).
[17] C. W. Shih and C. W. Weng, Physica D **146**, 213 (2000).